Study of a MEMS fiber-optic pressure sensor based on Optical Interferometry

by

Pedro Cordero Meza

A thesis
presented to the University of Waterloo
in fulfillment of the
thesis requirement for the degree of
Master of Applied Sciences
in
Mechanical and Mechatronics Engineering

Waterloo, Ontario, Canada, 2017

AUTHOR'S DECLARATION

I hereby declare that I am the sole author of this thesis. This is a true copy of the thesis, including any required final revisions, as accepted by my examiners.

I understand that my thesis may be made electronically available to the public.

ABSTRACT

The main focus of this thesis is the development of a MEMS optical pressure sensor capable of giving real-time, accurate measurements to a mid-high pressure range.

Some traditional devices for acquisition of parameters such as pressure or temperature have proven to be insufficient to the demands of the markets of research and manufacturing. State-of-the-art sensing technology has led to the construction of more reliable configurations that push the limits of traditional devices. Using micro-machined components is a suitable approach for applications that show restrictions just as limited space, noise measurement or interference created by the inaccuracy of electronic components that are not suited to be in close contact with the sensing medium.

A study of the current optical based technologies revealed the current use of extrinsic Fabry – Perot interferometers in the fields of medical, biotechnological and industrial applications. Each field presents a general specific limitation, given the nature of its environment. These mostly include low pressure and temperature ranges, non-protected sensors or super sensitive, expensive devices.,

The operation of this sensor comprises a non-emissive, optically powered device that shows precision measurements and immunity to electromagnetic interference. Tested over a mid-high pressure range that shows a 20% improvement over the devices found in literature. This sensor is the result of the coupling of a multimode silica optical fiber, a MEMS pressure sensor with a thin silicon film and a stainless steel housing for packaging.

A theoretical analysis and response simulations were used previous and along the process of construction and testing of the device. This analysis was followed by an assessment on the materials that were suitable for the assembling of the device, plus the pertinent modifications for each component that allowed a proper coupling.

Several tests were done previous to the final assembly of the device, where calibration, alignment and limitations of the device were studied previous to determine the sensor's response. The experiments were done at the SimsLab of the University of Waterloo, using a pressure chamber with direct connection to the housing of the sensor to avoid pressure leaks.

The sensor's properties include a silicon thin film with a thickness of 34 micrometers, an optical fiber with a core diameter of 125 micrometers, protected by a ceramic ferrule to provide stability and rigidity to the fiber. The fiber is part of a coupler that splits the optical signal between the input and output beams. The output leg of the coupler then sends the information to an OSI (Optical Sensor Interrogator) which is a set of electronics that use a photo detector to break the light into its spectral

components, analyzing fringes and converting the photons into electrons which are digitized as a function of the wavelength and read out via a USB port into a host computer.

A LabView program then converts the optical response to a value in millivolts that can be directly related to the changes in pressure that are detected by the deflective silicon membrane.

A complete characterization of the sensor's response was carried out. An averaged sensitivity of 1.3768 mV / psi over a range of 0 – 100 psi was found. An accuracy of 1.25 psi per 0.1 mV was established. The Noise Equivalent Pressure measurement could to be neglected over the accuracy that is limited by the capacity of the electronics.

In summary, an Optical MEMS pressure sensor was developed. This device is capable of being tested in laboratory and manufacturing-like simulated environments.

The pressure measurements acquired during this project assisted the base for a future prototype to be developed in enhancing the pressure range in a harsh environment, with elevated temperature. Proof-of-concept data was gathered and analyzed so further advances can be reached on micro-fabrication and optical techniques.

Acknowledgements

I would like to thank my supervisor Dr. Patricia Nieva for her support and guidance during the entirety of my degree, for instilling within me research abilities, analysis and critical thought that made this work possible.

Secondly, I would like to thank my colleagues at the SIMSlab; Axel Navarrete for his moral support and Eric Brace for his technical support and companionship during the project; and I would like to especially thank Abdul Rahman Ghannoum, whose support was fundamental to advancing my project.

Finally, to the University of Waterloo and the government of Ontario for the funding and financial support that allowed me to complete my graduate studies.

Dedication

To my family, for being my voice of reason and always believing in me, kept me moving forward.

Table of Contents

List of Figures

List of Tables

Chapter 1

Introduction

Conventionally, a sensor is an electronic component or device that focuses on the detection of a specific parameter(s) in its environment. It then sends the parameter information to another set of electronics that can process, transform and further analyze the information, and environmental context in which the sensor is working.

Depending on the application, these sensors need to have different characteristics and capacities that allow them to perform within their targeted objective.

Nowadays, sensing technology has improved enormously, illustrated by devices that are more accurate, more precise, and more sensitive to the acquisition of their intended parameters. However, even this improved technology has limitations in its capacity to deliver quality readings when exposed to harsher environments, such as higher ranges of pressure and temperature. This technology requires the aid of state-of-the-art optimizations including smaller operational sizes, and separation of the electronics from the sensing medium in which the sensor needs to operate.

In the interest of coupling leading edge electronics with state-of-the-art sensing technology, Micro Electro Mechanical Systems (MEMS) sensors have been a dependable solution in recent years. With the aid of existing techniques, such as optical interferometry, MEMS sensors are increasing their reliability and accuracy while saving space and lowering cost.

1.1. MOTIVATION

This thesis is motivated by the lack of reliable, robust, and cost-effective MEMS devices that can operate in harsh environments, The proposed approach includes the pairing of MEMS technology and optical-based Fabry-Perot (FP) interferometry. The advantages implemented by this pairing include reliability of measure, increased accuracy, cost efficiency, and smaller scale capacity. With correct packaging, this presents real-time output readings, without sacrificing robustness. To address this motivation, this thesis develops the capacity of MEMS optical pressure sensors within the context of controlled laboratory conditions as well as manufacturing-like conditions.

Fast responding sensors, based on optical interferometry are available among the literature [1], [2], [3], [4], [5]; however there is no clear evidence that similar devices are able to reach mid-high pressure ranges. This extended range is not generally required within the primary targeted fields of medical or biotechnical research.

The methodology this thesis applies includes a theoretical analysis, the study and selection of materials, assembling process and testing, and proper packaging. This combination is used to increase current pressure ranges for this type of devices.

1.2. OBJECTIVES

The objective of this thesis is the development and study of a MEMS optical pressure sensor that works on the principle of Fabry-Perot interferometry and can achieve mid-higher pressure measurements than its counterparts. This sensor implements the advantages of fiber optics in combination with thin film deflection and provides a short-time response.

The MEMS optical pressure sensor is designed specifically to achieve the following sub-objectives:

- Study and assemble a pressure sensor that shows reliable and accurate measurements.
- A 20 % improvement as compared to the pressure range of similar devices reported in the literature.
- Design of a straightforward and uncomplicated device that allows modifications and corrections for further prototyping.
- Development of a customized package to protect the fragile MEMS device and allow for adequate handling.

1.3. ORGANIZATION OF THIS THESIS

This thesis is comprised of six chapters: an introduction, a literature review, a theoretical analysis, two chapters containing product development, and a conclusion.

Chapter two presents background information on pressure sensors, followed by a definition of the basic principles of Optical Interferometry. The chapter focuses on the Fabry – Perot interferometer, supported by a literature review on state-of-the-art FP pressure sensors, which have been reported to operate on similar principles as the device built for this thesis. Distinct differences are identified through the examination of failure mechanisms, and study of assembly techniques, prior to the design and construction of this sensor. This chapter is concluded by a review of pressure sensors tested at higher temperature ranges.

Chapter three includes the theoretical analysis, which informed the construction of the device. The most relevant characteristics that enable this device to be functional are highlighted. Operational ranges and limitations, measures and outcome expectations are identified.

The theoretical analysis validated the research and selection of specific materials intended to deliver the required objectives and sub-objectives.

Chapter four presents the working conditions, requirements and constraints of the device. The material selection process used in the construction of the proposed MEMS pressure sensor is outlined, followed by the execution of pertinent modifications This chapter concludes with an explanation of the main failure modes that were present during the testing phase, and how they were used to correct and implement a functional device.

In chapter five, the final assembly is presented along with the experimental results of the device. This chapter includes a characterization and description of the sensor's properties. It expands the description indicating how the pressure trials were performed and how the acquisition system couples successfully with the MEMS pressure sensor and the optical fiber.

Finally, chapter six summarizes and lists the main contributions of the work presented in this thesis, proposing future steps to continue with the second prototype.

Chapter 2

Background and Literature Review

This chapter presents an overview on pressure sensors, transmitters and transducers, a pertinent background on optical interferometry as well as a comparison of different available techniques to combine with MEMS pressure sensors and why a Fabry – Perot was chosen. The essential background in order to understand the specifics of FP theory; a variety of different MEMS optical pressure sensors based on FP interferometry whose working conditions, device's performance and packaging methods, are worth comparing with this project, specifying clear differences and evaluating how could they have improved; lastly, a quick mention on dual-functional MEMS optical sensors and pressure sensors tested at higher (than room temperature) temperature ranges.

2.1. PRESSURE SENSORS

Due to the harsh environment in which they are used, general-purpose pressure sensors have to be really robust and are mostly dependable on mercury-based principles that actuate to temperature changes [6], [7]. Having this risky condition for the human being, has motivated the study of different technologies that can spare the fluid filled systems, the electronics in close contact with the sensing medium (which are likely to present failures when affected by higher temperatures), and that can manoeuvre in all kinds of environments and spaces, but at the same time adjust to the already stated testing mechanisms.

Commonly, current devices have their transduction mechanism is based on a Wheatstone bridge strain gauge that transmits pressure via fluid displacement. They are encapsulated in a stainless armour coating that provides thermal isolation and designed to be easily mounted or installed into most manufacturing lines that require pressure sensing under harsh environments [8].

From the emerging need to migrate from mercury-based devices to innovative arrangements, preserving the ability to function close to the plastic melt but at the same time, combining the benefits of MEMS pressure sensor and optical interferometry that use light to transfer data with low signal attenuation, a relative simple and robust structure and high accuracy and good sensitivity based on a micro membrane deflection.

2.2. OPTICAL INTERFEROMETRY

Sensors that work with optical interferometry serve to measure reflection and transmission (emission) of light, comprehensive of a wide range of wavelengths in both single and multi – mode fibers [2]. Conventionally, their functioning requires a beam of light, a fiber to transport it and a setup at one end of the polished fiber where the light will interact and later on, be analyzed. The light is regularly divided into two or more partials rays, with different (or equal) amplitudes depending on the application; each beam is directed through a different path-length with a specific refractive index, which is a property of the mean where the light is traveling in (the core of a fiber, air, water, vacuum); later on, they are all superimposed and directed to a detector that will interpret the incoming ray of light and will analyze the fringes, intensity, frequency, etc. Due to the fact that all beams come from the same light source (in most cases), intensity can be added or subtracted, as long as the phase does not surpass the coherence length. The total amplitude (intensity) of the light is dependent on the wavelength λ [9].

To achieve a more intense signal through the system, whether the light is jumping from one fiber to another, or it is being reflected from a surface, or light is being absorbed from a medium, all partial waves must interfere constructively.

Optical pressure measurements have been categorized into different detection and interferometry methods [10], we can find:

- Optically emissive, thermally powered: They do not depend upon an optical light source, but could present lack of measurement stability; frequent applications include detection of high temperatures (> 600 °C) [9].
- Optically emissive, optically powered: Require en excitation light source, generally are a fluorescence time rate of decay sensor, amongst the main advantages of this sensor we find a great reduction of sensitivity to source noise, but can be more complicated with the data acquisition system, and have limited temperature range [10].
- Non-emissive, optically powered: Changes in temperature are wavelength encoded onto the spectrum of a white light source, usually a Fabry – Perot (FP) interferometer helps to this purpose, mainly are single-mode devices [10].

Different options inside optical interferometers are available to use as demodulation system in combination with a pressure sensor, such as the Michelson Interferometer, a beam splitter is located at a certain distance from the light source, usually with a negligible absorption ($R + T = 1$), the two separated beams are reflected at two individual mirrors (M_1 and M_2), the beams are then directed into a third path of detection of intensity, this interferometer is not able to detect rapid oscillations with

frequency which makes it non ideal for high sensitivity pressure detection. As light will suffer substantial loses when being reflected and superimposed in the end, regularly a compensator plate is placed in one side arm of the device (output leg). The main uses for a Michelson Interferometer can be a filter for transmitted light, a mode selector for lasers or a wavelength-selective reflector [11].

Comparable to the Michelson Interferometer, the Mach – Zender works with constructive interference of two beams that were previously divided off of an incident light, the two waves travel through different paths with a phase shift; the main difference lies with a transparent object that is inserted into an arm of the device (no difference in which one, depends on the application) that will deliver a change in the wave's pattern that allows a high accuracy determination of the refractive index of the particular materials that form this device; the high level of sensitivity that can be achieved with this approach makes it ideal to analyze refraction of light. This type of interferometer has a great range of applications in spectroscopy matters such as measuring of refractive indices of certain vapors and their response when exposed to light patterns, also used for gas flow analysis or variation of density; but are generally comprehensive of calibration of the plates and the mirror like surfaces interacting with the light which could represent an important drawback if the reflecting surfaces need optimization during tests.

The most suitable type of interferometer for this application, due to capability of multi-tasking, high resolution and sensitivity, no electro-magnetic interference and robustness of the system, is the Fabry – Perot etalon.

2.3. FABRY – PEROT INTERFEROMETER

A Fabry – Perot interferometer is a linear optical component designed with two parallel reflecting mirrors separated by a gap (cavity distance); a particular ray of light incoming from one of this mirrors will make several round-trips inside the cavity creating a large number of reflections; an interference pattern will emerge with such a structure [12]. A FP interferometer depends highly on normal incidence and only certain wavelengths will resonate inside the cavity. If the reflected beams are in phase, constructive interference will be created giving a high-transmission peak of the resonator, for this to be fulfilled, the condition $L = m\frac{\lambda}{2}$ must be satisfied, where L is the distance between the two mirrors, m is an integer and λ is the wavelength of the light that travels inside the cavity; if the transmitted beams are out-of-phase, a transmission minimum will occur due to the phenomenon of destructive interference. These are variables that depend on the wavelength, the angle of incidence in which the light is reflected / transmitted, the indices of refraction of the mediums where the light is

traveling (*n*), the free spectral range (FSR) that depends on the separation of the mirrors and can be altered to change the oscillating modes (waves) that fit into this cavity [12].

The interference pattern is directly modified by a change in distance (*d*) inside the cavity; therefore, a deflective membrane with loaded pressure can be employed to vary the value of "d" to detect the variation of the reflected or transmitted oscillating modes due to the shift of this gap.

Taking advantage of the characteristics of a MEMS pressure deflective membrane in combination with the benefits of optical demodulation, an array in which a multimode optical fiber (that transports the light) is fixed to serve as the first surface, the micro-membrane poses as the second reflective surface and the light is shone between them.

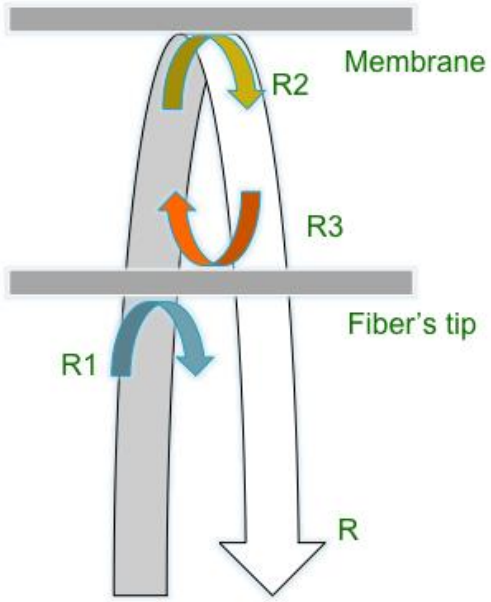

Fig. 1. Fabry-Perot interferometer concept.

Figure 1 represents how the path of the light inside of the system behaves, an incoming beam of light travels through a coupler to find exit at the fiber's tip, at the moment it exits the fiber, a factor loss *(V)* starts adding up every time the light encounters a new barrier for transmission or reflection.

The most notable reflection interactions are as follow:

- R_1: Incident light partially reflected at fiber's tip
- R_2: Incident light reflected at membrane
- R_3: Reflected light at the outside line of the fiber's tip (negligible)
- R: Reflection that goes back into the fiber

The intensity of Reflection (R) will travel back through the coupler and into the photo detector to analyze the phase difference between the input and the output amplitudes, the result gives a sinusoid with a peak-to-peak amplitude and offset that is dependable on all the previously mentioned factors (relative reflections, change in "d", angle of incidence) [13].

Acquisition of pressure measurements using MEMS Fabry – Perot sensors

The goal of this project is to develop a fast-response, real-time measurement pressure sensor with a higher pressure range than those presented in the literature, without neglecting the cost of fabrication (assembling of the components), the robustness of the final device and the accuracy of the readings.

A review is presented comparing some state of the art MEMS FP pressure sensors where their method of construction, optical interferometry and ranges of operation are compared with our device, highlighting that the pressure ranges fall short in comparison with our device. This may be accounted due to the fact that most of these sensors, are aimed for experimental use only, or applications such as medical use where the required pressure doesn't necessarily be higher that 50 psi. In addition, our sensor has a protective packaging comprehensive of a ferrule and a stainless steel tube that seal it on the inside, permitting higher ranges of pressure to be explored.

2.4. OPTICAL PRESSURE SENSORS

Pressure sensor fabricated on an optical fiber

Don C. Abeysinghe et al. [3] at the University of Cincinnati developed a FP pressure sensor which main difference with other devices is the fabrication of the membrane on top of a commercial optical fiber, eliminating the need for adhesives of packaging. This sensor withstood the capability of working up to the temperature of operation of the fiber (600°C). It is able to operate in smaller spaces, originally aimed for the medical industry. The idea was to create an alternative to current optical sensor fabrication methods. The final diameter of the device is that of the fiber, experiments were made with 200μm and 400μm diameter optical fibers. A broad band-light emitting diode was routed onto the sensor through a coupler (1x2), the reflected light was directed to a photodetector that later converted the intensity of light into voltage [3].

The main limitations that this sensor has, is that due to the nature of the fragility of the fiber, it could only be used in a controlled lab environment, with static pressure. It didn't show a liner response with several acquired points (which could be accounted to the fabrication process and an uncompensated

deflection that surpasses the Young modulus of the membrane); another major difference with Don C. Abeysinghe's sensor and the one developed for this project, is that his device can only operate and sense lower pressures, from 0 to 80 psi, falling short in comparison on what the current approach for this project is looking for (100-200 psi). This issue rises from the theoretical nature of using just a fiber as the main body of the sensor, and could be improved by protecting the fiber with a ferrule or canulae, leaving the tip exposed as safely as possible.

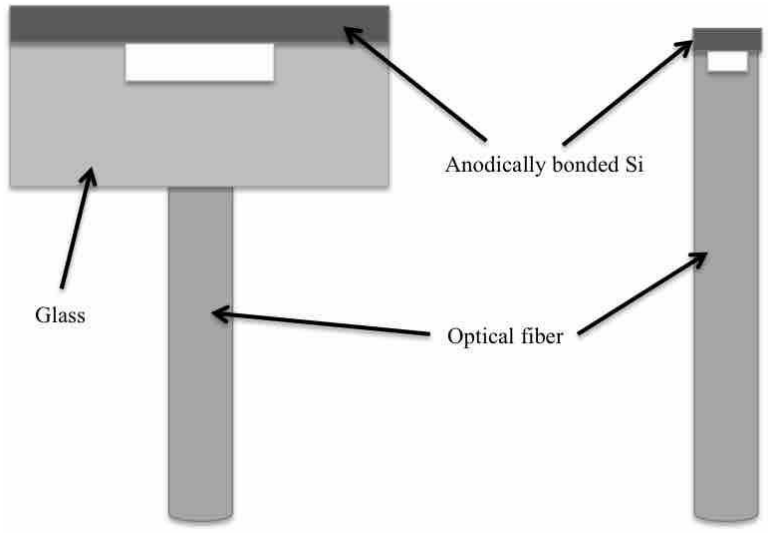

Fig. 2. Schematic of different structures for fiber optically interrogated MEMS pressure sensors. (a) Represents a typical configuration comprehensive of a glass plate with a thin silicon diaphragm anodically bonded to the wafer. (b) Represents the customized configuration presented by Don C. Abeysinghe [3] where the Silicon membrane is on top of the optical fiber.

High Sensitivity FP interferometric pressure sensor based on silver diaphragm

Switching from silicon / silica to silver as the membrane's material was the approach taken by Feng Xu et al. [4]. The idea was presented due a higher cost of fabrication when using Silicon for the microfabrication process, compared with the design of a Silver diaphragm.

This sensor has a thickness of just a few of micrometers (1.5μm to 1.6μm thick). Silver was selected as the reflective surface due to the stability shown when deflecting, along with high reflectivity for light (between 90% and 96% of reflection with a centered wavelength of 1550 nm).

This sensor was built with a single mode fiber with a core diameter of 125μm inside a zirconia ferrule used for both protection and also as the FP cavity. Taking advantage of the strong inherent adhesive force of the membrane, it can be heated up to a temperature of 75°C and stick to the ferrule's tip. On

the other end, the space between the ferrule and the fiber is sealed using a curing epoxy adhesive; tests were made using static pressure inside a pressure chamber to adjust different values and achieve a linear response [4].

The tests were made using a range from 0 to 8 psi, in which a good sensitivity was shown, (70.5nm / 0.14psi). When comparing to a Silicon diaphragm like the ones listed in this review, it improves the sensitivity by 14% - 20% in average; which is explained by how thin the membrane of this device is. The sensor cannot be tested in high temperatures (anything beyond 45°C), the diaphragm was fabricated and attached to the ferrule which trapped air inside the FP cavity, this caused a thermal expansion provoked by air during the experiment when it wasn't at room temperature. In comparison with the set up proposed by our device, changing the diaphragm to a metal-based material would increase the reflectivity of the membrane, it may lower the cost of fabrication. The main drawback is again, the pressure range and low temperature dependence of their experiment, as it cannot be used for harsh environment, which is one of the aims of this proof of concept. Increasing the diaphragm's thickness would create more of a dependence on temperature and although it may work at higher pressures, will still start failing at anything beyond 45°C.

FP pressure sensor with a 45° angled fiber

H Bae et al. [5] worked on a cross-axial FP sensor that can provide measurements of static pressure and compensate the dynamic pressure stimulus that the device could be subjected to when real time testing inside a specific flow of oil (which was described as the main application). To achieve this purpose, they polished the fiber to a 45° angle and placed the fiber's tip parallel to the membrane, so that one of the mirrors is the bottom of the membrane and the second mirror if the side of the fiber. This arrangement allows the use of the sensor in a continuous-flow environment where the sensor is not entirely fixed in one position.

A single mode fiber was employed and a polishing machine to ensure the correct angle for the tips, they required an initial batch of approximately 35 fibers; additionally, a thin layer of silver was evaporated onto the end face (thickness not specified), to enhance reflection.

A 2x2 coupler was used as part of the demodulation system and the final thickness of the diaphragm is 18 μm. The pressure range for testing comprehended from 1.9 to 14.2 psi, showing a reliable sensitivity of 0.009 μm / psi.

The sensitivity was achieved through carefully controlled cavity distance (13.8 μm) that allows this type of interferometry to respond in real time to the nano-metric changes in the membrane's deflection.

Likewise, this device was designed to operate at a lower pressure range in comparison to the one presented in our project, and based on the author's comments, calibration was rather complicated, not to mention that it can only operate reliably up until 40°C, due to the lack of a protective packaging for the fiber.

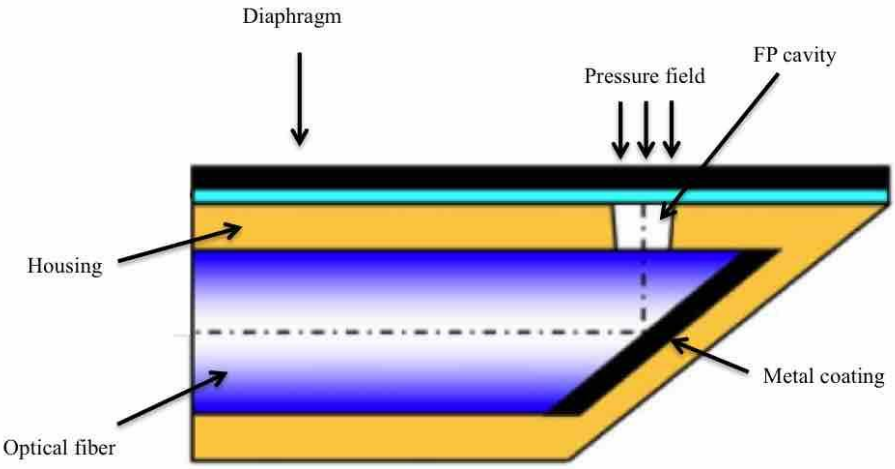

Fig. 3. Schematic of the pressure sensor with cross-axial configuration. Modified from [5].

2.5. MEMS OPTICAL PRESSURE SENSORS TESTED AT HIGH TEMPERATURES

MEMS FP chip for simultaneous pressure and temperature sensing

Cheng Pang et al. reported on a successful implementation of an optical system that can provide simultaneous measurements of pressure and temperature within a single device. It allows these analyses based on two principles: a silicon membrane that responds to pressure stimulus and deflects, and a cavity that changes size when temperature changes occur and thermal expansion modifies the cavity's size.

Unlike the common construction of a FP cavity based interferometer, this one was constructed using two reflecting surfaces (both silicon) in the shape of an "L". The optical fiber is set parallel to the silicon membrane (which actuates as the deflecting surface to detect pressure) rather than perpendicular so that the light has a normal incidence on the membrane. To make this set up work, a microfabrication process was used on two silicon wafers (upper and lower parts of the sensor), using thermal oxidation and etching for the cavities. After the shapes were created, a silicon-to-silicon fusion bonding process was utilized. An optical fiber was polished to a 45° angle and attached to the

inside hole designed to hold it; it was put inside with the guidance of an optical profilometer and sealed with a high temperature endurance epoxy (up to 300°).

The fiber is connected to a coupler that has a 50% / 50% splitter, one end goes to a second splitter that connects a FP tunable filter (used to modulate the wavelength used in the experiments) and to a Superluminescent Light Emitting Diode (SLED) which provides the light. The first splitter is connected in one end to a photodetector.

To have a better reflectance on the two surfaces where the light is going to hit and bounce, a thin metal layer was sputtered on top of the surfaces to increase the refractive index and intensity of the signal.

The functioning of this device requires a rather complicated calibration system and it can be easily affected if the orientation of the fiber changes, as they used a parallel sitting for the fiber, the 45° angle permits the light coupling when the ray hits the second surface and send the beam back to the fiber [1].

Although the results of the experiment show a linear response to changes in pressure at room temperature (26.1°C), an important variation shows when the temperature goes up, the sensor was tested at a maximum of 250°C presenting between 5% and 10% of difference with simulations previously done, and the range of pressures that were used go from 1.7 to 60 psi. This implies that this arrangement is not ideal to perform pressure and temperature sensing in harsh environments; it presents a complicated process of construction and calibration, and depends on the correct positioning of the fiber, so another main disadvantage is that it lacks robustness.

MEMS FP pressure sensor for high temperature application

Among the sensors that have been reported in the literature, one that shows prominent results closer to what the main goal of this project is, is the work developed by G. C. Fang et al. as they integrated a device that works on the principle of Fabry Perot interferometry for pressure sensing at high temperature ranges (from 20°C - 300°C) [14]. Among the main advantages of this device, we find a good sensitivity to pressure (tested pressure range goes from 0 to ~ 88 psi), that diminishes a bit every time the temperature goes up, they reported a value of 0.24 nm / psi when exposing their device at 20°C. This type of sensitivity can be used for medical devices when sensing blood flow or other types of thin liquid-immerse applications. The sensor's sensitivity is directly related to the finesse of the device, which will be explained on section 3.3; it means the FP cavity where the light resonates, has low indices of refraction and more intensity of light gets reflected back and forth creating constructive interference in their device, this is all accountable to the materials that they used while assembling

the device, they sputtered a layer of gold beneath the silicon membrane that enhanced the reflectivity within the cavity.

The sensitivity and the accuracy of the device does decrease once the temperature increases, it reportedly goes down to 190 nm / psi when reaching 300°C which represents a shift of almost 800% from room temperature. The sensor also loses linearity due to the thermal drift. Although it is not clearly stated, the research done in FP sensors' fabrication indicates that the setup employed in this project may not be suitable for industrial production, which is one of the goals of this thesis.

Chapter 3

Theoretical analysis

In this chapter, a theoretical analysis is done. It describes the physics of the Fabry – Perot interferometry, starting with the Airy functions that allow a comparison between materials properties and intensity of reflection, which is the base principle of the device. It goes over the response of the light inside the system and how the light inside the FP cavity creates constructive and destructive interference that results in a change of the initial intensity.

Followed by an analysis and inclusion of the optical losses, how the device's finesse (sensitivity) will affect the readings and performance of the setup. This analysis assumes normal incidence of the light, perfect parallel mirror-like surfaces and a plane wave beam.

To conclude, a theoretical analysis of the mechanical deflection of the silicon membrane.

3.1. FABRY – PEROT SUMMARY

The Fabry – Perot interferometer works on the principle of amplitude division of electromagnetic waves [15]. An incident beam with Intensity (I_0) is transmitted from a medium (the optical fiber, in this case) with a reflection coefficient r_1, the transmitted beam enters into a cavity with a certain length (l_0) in which the beam is reflected and transmitted between two surfaces (ideally, mirrors). The beam resonates inside the cavity creating several round trips, and then gets transmitted back into the first medium (the optical fiber) where a different intensity (I_1) travels back into a photo detector.

Inside the FP cavity, a round trip occurs when the incident ray is incident in the first reflecting surface with amplitude coefficient r_1' after propagating twice the cavity distance ($2l_0$). This creates an interference between the reflected fields $E_{r,2}$, $E_{r,3}$, $E_{r,4...}$ that are transmitted and reflected from the electric field $E_{r,1}$.

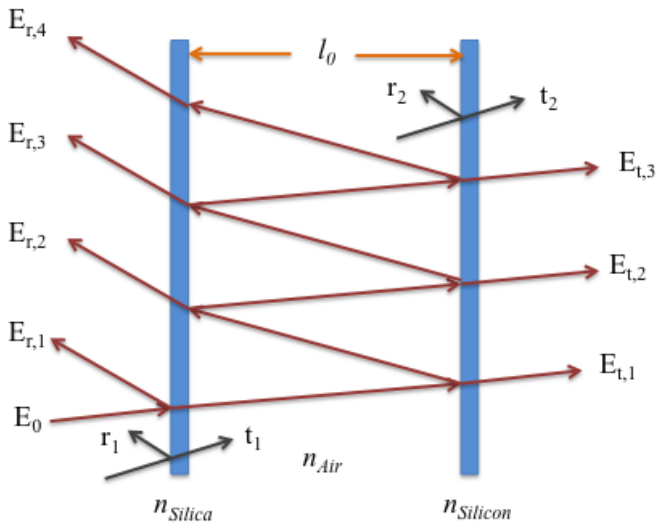

Fig. 4. Fabry – Perot interferometer formed between the tip of a silica fiber and a silicon membrane. Showing reflection and transmission coefficients r_1, r_2 and t_1, t_2, respectively.

The structure of a planar Fabry – Perot interferometer is shown in Figure 4, it depicts both reflecting surface's coefficients and the indices of refraction of the elements involved in the system.

The incident beam with initial intensity I_0 is presented in its electric form as an electric field E_0, which is incident on the FPI; for the case of this device, a planar wave analysis is assumed, with non – diverging beams. The electric fields that are reflected of surface 1 are superimposed into r_1, and interfere with the summation of the electric field of surface 2 that has amplitude r_2. This behaviour can be analyzed with the Interferometer Transfer Function in terms of the phase ϕ, ITF_ϕ.

The electric fields that travel inside the cavity have a complete round trip when the condition $2ml$ is fulfilled, where:

- m = round trip number
- l = cavity distance (after suffering alterations)

The final summation of the electric fields that have traveled the cavity distance twice (hence the 2 in the previous formula, due to the round trip), can be expressed as [15]:

$$E_{Total} = r_1 E_0 e^{i(kz-2\pi ft)} + \sum_{m=0}^{\infty} t_1 t_1' r_1'^{(m-1)} r_2^m E_0 e^{i(kz-2\pi ft)} \qquad (1)$$

Whether the FPI will create constructive interference (augmenting intensity) or destructive interference depends on the ability of the FP cavity to retain energy, which is directly dependent on the total internal reflection R [16]. Each cycle of the waves creates a peak, as the reflectivity increases, the peak becomes narrower and as the reflectivity decreases, the peak will be broader.

Constructive interference will be shown when the condition in equation (2) is fulfilled:

$$\frac{p\lambda}{4} = nl \qquad (2)$$

Where:

- p = integer

Contrary, destructive interference results when $p = 1, 2, 4, 6\ldots$ m for the expression:

$$\frac{p\lambda}{2} = nl \qquad (3)$$

For the analysis of this setup, where the refractive index of air (n_{Air}) is 1 and the wavelength is 850 nm, every time the cavity distance shifts to multiples of a quarter of the optical thickness, constructive interference is created. Opposed to destructive interference that occurs when 850 nm is multiples of half the optical thickness.

3.2. SIGNAL DETECTION WITH OPTICAL FABRY – PEROT INTERFEROMETRY

The materials that were picked to assemble this setup have direct impact in the reflection and transmission that the system suffers; the behaviour of the sensor is firstly affected by the refractive indices (n) of the reflecting surfaces. Refractive index can be defined as the factor when light reaches a certain medium, the capability this medium has of reflecting or absorbing the light, depending on density; the lower the refractive index, more light gets reflected back [9]:

$$n = \frac{C}{C_s} \qquad (4)$$

- Refractive index of Air: 1
- Refractive index of Glass: 1.5
- Refractive index of Silica: 1.4565
- Refractive index of Silicon: 3.42

The ideal Fabry – Perot interferometer assumes no transmission (t_1, t_2) or absorption of the system, nonetheless, the high indices of refraction of the materials involved in this setup, plus the transfer medium being air and not vacuum, generates a significant amount of loss of the system, which has a direct impact in the sensitivity of the pressure sensor.

Reflection, transmittance and absorption losses = 1 [17]. Depending on the instrument's application, these factors can be modified with help of the refractive indices of the materials being used, the FP cavity's distance "d", the wavelength and the intensity of the light.

Reflection coefficients can be defined as the power of reflection that each mirror has taking into consideration the refractive indices of the materials involved [18]:

For the analysis of reflection, the system is divided into 2 sectors, and each one is calculated as follows:

- Sector 1, where:
  - R_1: Reflection coefficient at fiber's tip (Silica)

$$R_1 = \left(\frac{n_2 - n_1}{n_2 + n_1}\right)^2 = \mathbf{0.0345} \qquad (5)$$

  - Reflected back into the fiber (at fiber's tip): **3.45 %**
  - Transmitted into medium – air (also known as Fabry – Perot cavity): **96.54 %**

- Sector 2, where:
  - R_2: Reflection coefficient at membrane (Silicon)

$$R_2 = \left(\frac{n_2 - n_1}{n_2 + n_1}\right)^2 = \mathbf{0.2997} \qquad (6)$$

  - Reflected from the membrane, back into the fiber: **29.97 %**
  - Transmitted into medium (loss): **70.02 %**

Total Reflectance can be calculated as [15]:

$$R = \frac{\left(\sqrt{R_1} - \sqrt{R_2}V\right)^2 + 4\sqrt{R_1R_2}Vsin^2(KL)}{\left(1 - \sqrt{R_1R_2}V\right)^2 + 4\sqrt{R_1R_2}Vsin^2(KL)} = \mathbf{0.3715} \qquad (7)$$

- Reflectance of the system, after the interaction with the two reflecting surfaces that form the Fabry – Perot resonator: **37.15 %**

Total Transmittance:

$$T = \frac{(1 - R_1)(1 - R_2)V}{\left(1 - \sqrt{R_1R_2}V\right)^2 + 4\sqrt{R_1R_2}Vsin^2(KL)} = \mathbf{0.5984} \qquad (8)$$

- Transmittance of the system, after the Fabry – Perot setup suffers losses from the interference of the beams and the refractive indices of the mediums involved: **59.84 %**

This device shows a high percentage of intensity transmitted through the reflecting surfaces that are involved, which means that the initial intensity shone from the LED will undergo substantial losses.

A traditional Fabry – Perot signal consists of sinusoidal waves with repetitive oscillations, the amplitude of the wave corresponds to the change in distance from the two reflecting surfaces, and one complete wave occurs after the device has a shift of 850 nanometers, which will happen after a total amount of 6094 psi.

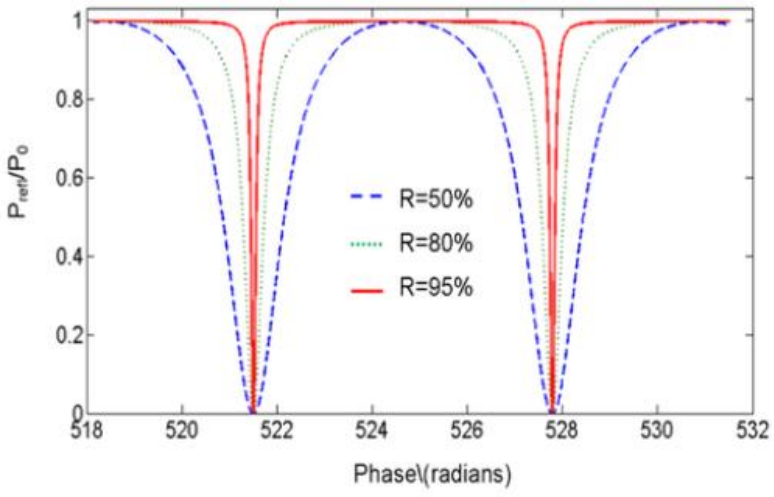

Fig. 5. Change in cavity distance of a Fabry – Perot pressure sensor at different reflectivities (50%, 80% and 95%). Change of pressure vs. Phase difference. Extracted from [19].

Figure 5 shows the behaviour of the FP interferometer for different total reflectance percentages. The relation between the increase of the surfaces' reflectivities and a narrower the shape of the peak is linear, it is due to the capacity that a FPI has of reflecting and retaining the light.

For this setup, the reflectance percentage is 37.15 %, which makes the peak wider than the one showed in figure 5 for 50%, this means that the frequency presents a delay and the shape will be less inclined. It also represents that the system has a greater amount of loss derived from the transmission and the absorption losses.

To estimate the amount of energy loss involved in the system, it is necessary to analyze the influence of absorption losses, given by the equation (9) [12]:

$$A = 1 - R - T \qquad (9)$$

$$A = 1 - 0.5984 - 0.3715$$

$$A = 0.0301$$

This means that an extra 3.01% of energy is absorbed inside the system, each of the materials involved in the setup has a different energy absorption coefficient that are listed in the table below.

Table 1. Absorption coefficients.

Wavelength	Material	Absorption coefficient (μ)
850 nm	Silicon	1000 cm^{-1}
850 nm	Glass	90 cm^{-1}
850 nm	Air	1.64 (MHz * cm^{-1})
850 nm	Silica	960 – 980 cm^{-1}

The coefficient for the loss of light described in table 1, can be seen as a block of the reflected light that gets transmitted into the medium where it collides, which constitutes absorption; it is given by what is called effective cross section (σ [cm^2]) that is affected by the constant denominated absorption efficiency Q_a (dimensionless) [20]:

$$\sigma_a = Q_a A \qquad (10)$$

The absorption coefficient is then calculated from the volume density of the medium where the light is being transmitted, by the cross-sectional area per unit volume of this specific medium.

$$\mu_a = \rho_a \, \sigma_a \qquad (11)$$

However, the loss per round trip of a FPI that assumes normal incidence, can also be approximated using an empirical relation, according to the formula [21]:

$$\Delta V = \exp\left\{-\alpha N_{eff}^{\beta}\right\} \qquad (12)$$

The parameter for α and β are detailed in the following table [9]:

Table 2. Parameters for α and β

R	0.0	0.2	0.4	0.5	0.6	0.7	0.8	0.85	0.9	0.95	0.99
Parameters											
α	5.1	4.3	2.84	2.46	2.18	1.86	1.5	1.34	1.18	1.05	1.02
β	2.69	2.46	1.91	1.83	1.84	1.81	1.58	1.46	1.35	1.12	0.84

3.3. SENSITIVITY OF THE FABRY – PEROT INTERFEROMETER

Sensitivity as an absolute quantity can be defined as the smallest amount of variation (absolute) that can be observed, noticed or detected by the sensing mechanism. Optical sensitivity is defined as the variation of the intensity of the reflected light per unit change (decrease or increase) in the FP cavity thickness [12]. Sensitivity is derived from the Airy model; as this device has high refractive index surfaces, the resultant total reflection (R) is lower than 90%, which categorizes the beam divergence into the ideal Airy function [22].

The optical sensitivity has a direct relation with the change in phase of a round trip of the light inside the FP cavity. The phase can be expressed as:

$$\phi = \frac{4\pi n l}{\lambda} \qquad (13)$$

Where:

- ϕ = phase
- l = cavity spacing
- n = refractive index
- λ = wavelength

The Airy function R is dependent on the phase shift that the beam suffers while interfering inside the cavity, it can be defined as:

$$R = \frac{F \sin(\frac{\phi}{2})^2}{1 + F \sin(\frac{\phi}{2})^2} \qquad (14)$$

Where:

- F = coefficient of Finesse [23]:

$$F = \frac{4R}{(1-R)^2} = \mathbf{3.7619} \qquad (15)$$

It depends on the coefficient of reflection of the mirror surfaces; it exhibits the resolution of the device. The higher the finesse, the lower the transmittance of the instrument, which makes it have a higher reflectance of the light inside the cavity.

For this specific calculation, the finesse is good enough to have a sensitivity of ~ 1.3 psi; by increasing it, the sensitivity of the system could be augmented, as there is a direct correlation between these two factors.

The closer the values of the reflection coefficients are for the mirror surfaces, the lower the mismatch will be (from 0 to 1) and the higher the reflectance inside the FP cavity, this number can be altered when using the same materials for the mirrors or special coatings to improve reflectance of the less reflective surface, mismatch can be calculated as:

$$M = \left(\frac{\sqrt{R_1} - \sqrt{R_2}}{1-R}\right)^2 = \mathbf{0.3312} \qquad (16)$$

Wavelength of light: Electromagnetic waves travel at the speed of light, frequency and wavelength are determined by:

$$f = \frac{c}{\lambda} = \mathbf{4.6121x10^{14}\ Hz} \qquad (17)$$

Where:

- f = Frequency in cycles per second
- c = Light velocity: 299,792,458 $\frac{\text{m}}{\text{s}}$

- λ = Wavelength in meters

The expression for optical sensitivity that comes from the Airy function is dependent on the change of phase, and its derivative form is expressed as:

$$\frac{dR}{d\phi} = \frac{Fsin\left(\frac{\phi}{2}\right)cos\left(\frac{\phi}{2}\right)}{1 + F\ sin^2\left(\frac{\phi}{2}\right)} - \frac{Fsin^3\left(\frac{\phi}{2}\right)cos\left(\frac{\phi}{2}\right)}{\left(1 + F\ sin^2\left(\frac{\phi}{2}\right)\right)^2} \qquad (18)$$

Finally, the optical sensitivity S_O can be expressed as the change in the reflected light *dR* at the maximum of the derivative of equation 19 with respect to the phase ϕ, and is defined as:

$$S_O = \frac{dR}{d\phi} \qquad (19)$$

Higher optical sensitivity can be achieved when smaller modulation in the derivative of phase ϕ results in the maximum variation in the reflected light dR. To improve the optical sensitivity, the immediate step would be to increase the mirror surfaces' reflectivities of the Fabry – Perot interferometer.

3.4. MECHANICAL BEHAVIOUR OF THE MEMBRANE

The pressure sensor that forms the FPI has a silicon membrane that deflects with stimulus on top of the thin film; the bending of the diaphragm is analyzed as a change of distance ΔL.

Total deflection (maximum deflection of a 34 μm thick membrane when applied maximum pressure, according to the sensor's specs for maximum supported pressure) can be defined as the relationship between a flat membrane center deflection and pressure stimulus ΔL [24]:

$$\Delta L = -\frac{Pa^4(1 - v^2)}{4.2Et^3} = \mathbf{-17.7\ nm} \qquad (20)$$

Where:

- ΔL = Center deflection of the membrane, when maximum pressure is applied
- P = Applied pressure (Pascal) = 689,476 Pa (100 psi)
- a = Half side length = $\frac{320}{2} = 160$ μm
- t = Membrane thickness = 34 μm

- E = Young's modulus = 150 GPa
- v = Poisson ratio of membrane material (silicon) = 0.17

The membrane is responsive to small changes in pressure, it can deflect to stimulus even smaller than 1 psi according to the supplier's specifications, however the sensitivity of the optical setup only allows detection of ~ 1.25 psi, when coupled with the photo detector. This is mainly due to the coefficient of finesse of the FPI, as explained on section 3.3. The change of cavity length dL per unit change in pressure dP [24] (Change in FP cavity distance "d" per 1 psi applied on top of the membrane):

$$\frac{dL}{dP} = -\frac{3a^4(1-v^2)}{16Et^3} = -\mathbf{0.1395}\,\frac{\mathbf{nm}}{\mathbf{psi}} \qquad (21)$$

Which means that per psi, the deflection the membrane will suffer is 0.1395 nm.

Received Optical Intensity (I_T):

$$I_T = \frac{R_1 + R_2 - 2\cdot\sqrt{R_1R_2}cos\phi}{1 + R_2R_1 - 2\cdot\sqrt{R_1R_2}\cos\phi} = \mathbf{0.2833} \qquad (22)$$

- The Resolving Power of the spectrum of light, depending on the reflection coefficients, the distance "d" of the cavity and the wavelength used.

After the Fabry – Perot setup is resolved, the resulting intensity of the output beam is **28.33 %,** after the reflection, transmission and losses.

The Free Spectral Range (FSR) is the wavelength separation between adjacent transmission peaks and is known to directly affect the finesse (F) of the system. The finesse is a factor given to quantify the performance of the resonator. Commonly, the finesse can be seen as the number of interfering beams inside the FP cavity; the higher number of interfering beams, the higher the finesse of the device, therefore, higher resolution measurements. The resolution of the device is mainly affected by the reflecting surfaces, as it has a direct impact on the number of beams that oscillating within the cavity.

Chapter 4

System design & fabrication

Chapter four includes the requirements and working conditions of the device.

This section details a list, description and justification of the material selection process. Additionally, the pertinent modifications and assembling steps followed to achieve a sub-assembly and a latter final device.

The mode of operation of the sensor is explained in further detail. To conclude, the malfunctions found present during the testing stage and how they were corrected in the final prototype.

4.1. WORKING CONDITIONS

In most pressure sensing applications, the responsive device is placed in closed contact to the sensing medium. Whether it is submerged in liquid, affected by air or vibration, it is often exposed to destructive conditions. As mentioned in section 1.2, the proposed MEMS pressure sensor will be coupled with optical interferometry to substitute the use of a mercury-based structure.

The use of oil or liquid to apply pressure to the membrane is simulated inside an air pressure chamber. Constant changes of pressure are controlled manually and the sensor is expected to read these variations.. The applied pressure is measured in real time and the experimental results of the demodulation system are compared to the theoretical principle of a FP etalon.

4.1.1. REQUIREMENTS

The MEMS pressure sensor – optical fiber coupling needs to be protected by a stainless steel housing that matches the specifications of current industrial products. Moreover, the installation of our system needs to fit the space and dimensions of standardized industrial manufacturing tools. At the same time, in account for the nature of the deflective membrane, it needs to be directly exposed to the air pressure so that the interaction causes the thin film to bend and give a change in the cavity distance “d” of the optical interrogator, which will cause an interference change of the light. The device needs to show a linear response, a direct relationship between to the augment of pressure and the increase

of voltage (which is how the signal of light is converted and read) as well as an expected sensitivity of 1.21 psi per 0.01 mV per 1 psi, according to the experimental results.

4.2. SELECTION OF MATERIALS & MODIFICATIONS

4.2.1. PRESSURE SENSOR

Silicon membrane based sensors are a state of the art alternative for monitoring of different parameters in various applications. For this project, silicon was chosen due to its properties of linearity, adequate coupling with optical interferometry, fast response and tolerance to harsh environments such as high pressure.

The sensor that was selected for this setup is the SE103, offered by BCM Sensor Technologies. It functions primarily as a Micro Electro Mechanical System (MEMS) piezoresistive actuator and its main applications are process control systems, biomedical instrumentation and automotive components. It is built as a silicon on glass structure with a sealed cavity for absolute pressure that had to be exposed from the back so that the optical fiber could shine the ray of light that interacts with the deflection of the membrane, switching to differential pressure.

The vent that was drilled opened provides just sufficient allowance for the ferrule that contains the fiber to make a tight fit and align to the center of the bottom face of the silicon thin film (refer to figure 6).

The SE103 offers high stability and precise linearity for accurate measurements that all together with the optical system, provide a resolution of 1.21 psi per 0.01 mV. The die has a footprint of 2.45 mm x 2.45 mm x 1.2 mm. The sensor is divided in a glass wafer with a thickness of 800 μm, a sealed cavity of 366 μm and a silicon membrane of 34 μm.

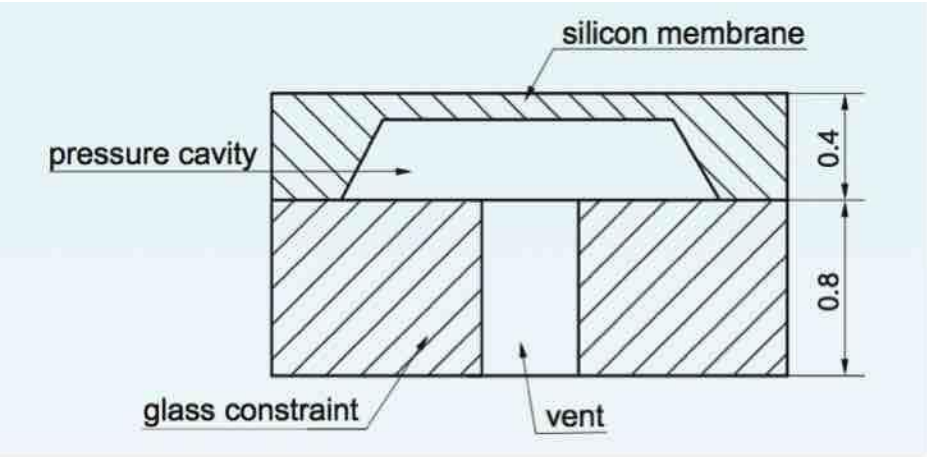

Fig. 6. Schematic cross section of the SE103, provided by BCM technologies and drilled to fit a ferrule containing an optical fiber in the middle. Extracted from [25].

The SE103 needed to be modified to make use of the reflective membrane. Reflection of the thin film allowed the analysis of pressure stimulus. The opening of a hole in the middle of the glass wafer permitted this study. The ferrule that was inserted into the sensor has an outside diameter of 1.25 mm; a tight fit + silicone (to immobilize the position) was the choice to fix the ferrule (once it was calibrated and set to a steady position within the sensor), aiming for the center of the thin film which is where the most amount of deflection occurs. The selected diameter of the hole is 1.3 mm, leaving a tolerance of 50 μm.

By design, the depth of the hole is 800 μm. This distance penetrates the glass entirely and reaches the cavity between the glass and the silicon membrane.

Creating a hole through glass required the following considerations: (1) a perpendicular hole; (2) a hole at the center of the sensor; (3) desired depth: 800 μm; (4) protection of the front side of the membrane to avoid scratching and damaging of the thin film.

Two options were studied. A comparison table is presented showing advantages and disadvantages of the available methodologies:

Table 3. Methodologies for opening a hole into the glass wafer.

	Advantages	Disadvantages
Glass drilling	• More control of the depth of the drill	• Debris and dust that contaminate the membrane

	• Diamond drill can penetrate through glass without breaking it • Low cost	• Hand made job
Laser engraving	• Cleaner cut • Repeatability of the exact spot of the cut	• Less control of the depth of the cut • No guarantee of the integrity of the membrane, once the glass is penetrated • Higher cost

A shop with experienced in handling of small pieces of ceramic / glass / diamond / metals was contacted to perform the modification: MT Jewellers and Goldsmiths.

Precision in location and protection of the front side of the sensor are needed, as these will directly affect the reflectivity of the membrane and the angle of refraction. A diamond drill with circular cavities built in its structure is the best option to penetrate through glass. It permits trapped air and debris to escape and this allows a much cleaner cut with significantly decreased visual contamination of the bottom of the membrane.

Once the sensors are drilled, the main concern was the cleanliness of the membrane. The pressure sensors were exposed to a cleaning procedure that consists of:

- Isopropyl alcohol bath for 5 minutes
- Drying of the sensors with a pressurized air gun
- 15 minutes inside the ozone cleaner to get rid of as mush impurities as possible
- A precision positioner probe (Cascade Microtech - DCM 210) to remove any big residual piece of glass remaining on the thin film.

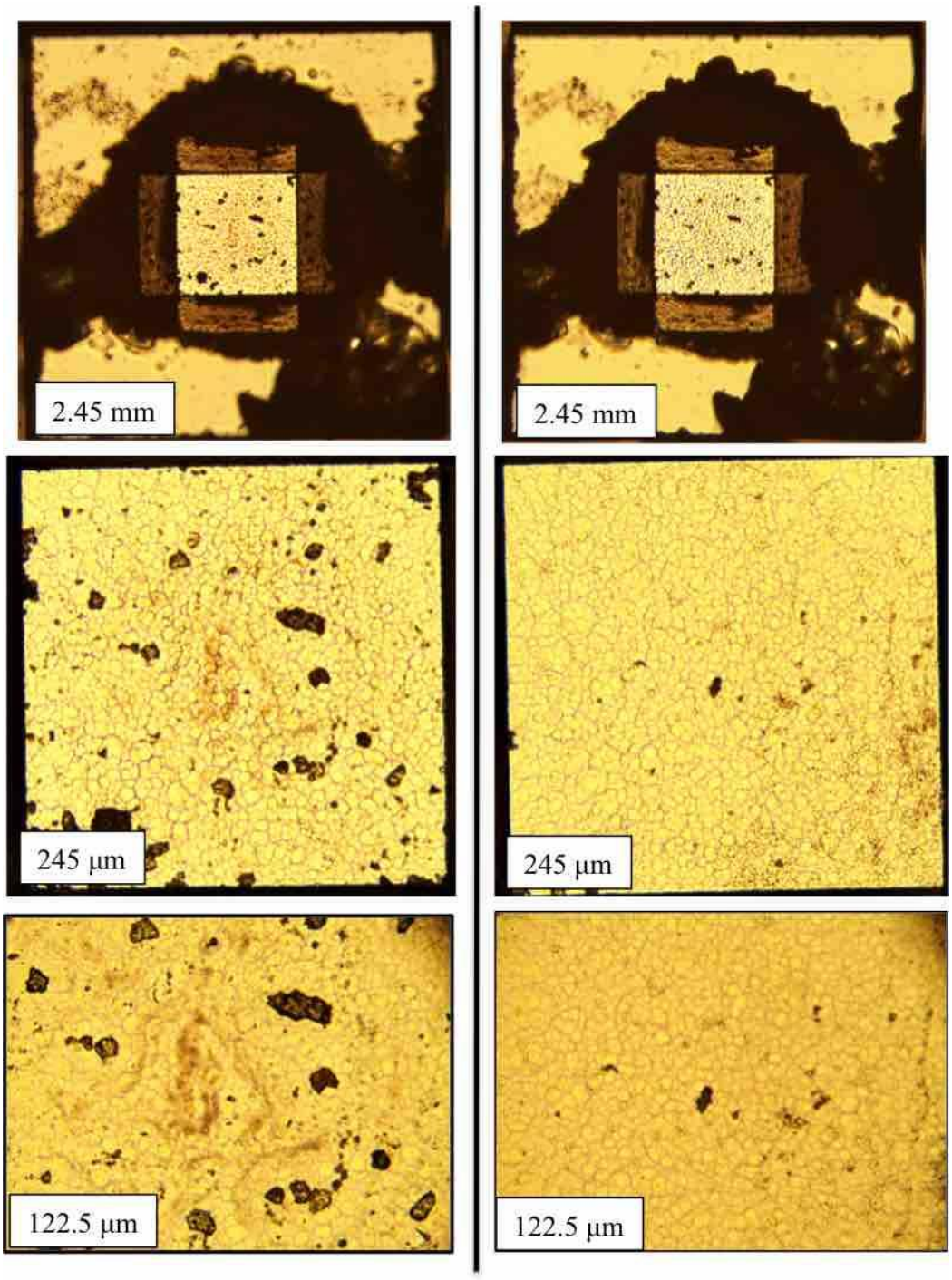

Fig. 7.Comparison of a membrane before and after being drilled at the center of the glass wafer and cleaned.

A stock of drilled sensor was kept at the SimsLab for experimentation and calibration of the device. Some of them were broken or shattered due to testing of the epoxy materials, positioning of the fiber and scratching of the ferrule against the silicon membrane.

The sensors need to be kept in a clean box to prevent contamination from the environment and debris to fall and get attached to either side of the membrane.

4.2.2. OPTICAL FIBER

Optical fibers are a commonly used technology for data transmission for all sorts of communication applications. They contain and transport light over different distances, depending on the specific use they are intended for.

Optical fibers present several advantages over other means of connection. These include: no heating (no thermal interference up until the operational temperature range), safe carriage of information, minimal loss over longer distances and certain bending is permitted (if bending is a consideration, a study of total internal reflection is needed [26]).

Typically, a fiber consists of a core with a high index of reflection that allows the light to bounce freely at the next barrier that is called cladding (preventing it from being transmitted to the outside). The cladding is usually made from a different material with a lower index of reflection that contains the light within, and a protective layer of coating to give rigidity and stability to the fiber. This third layer may not always be included in every fiber.

For this project, the GIF50C graded-index multimode fiber from Thorlabs was selected due to its properties that matched the requirements: (1) multimode fiber; (2) Numerical Aperture (NA) of 0.22; (3) 250 μm coating diameter to adjust the inner diameter of the ferrule (to be complemented in the following section); (4) flexibility to withstand tight bends with significant small loss; (5) low cost.

4.2.3. CERAMIC FERRULE

The ferrule that is used in this setup provides protection and stability to the fiber, alignment to the center of the membrane and a safer way of attaching the fiber to the structure of the sensor.

Thorlabs offered a 1.25 mm diameter ferrule that holds a 250 μm diameter fiber inside, it has a length of 6.4 mm and the fiber that sticks on the back has a length of 2 mm that had to be customized and attached directly to the coupler to prevent loss of intensity of light from an extra connection. It is also capable of bilateral stimulation, which means that light can be shone from it and at it with no need of an extra collimator. It fits well with the pressure sensor's wafer size (2.45mm by 2.45mm).

Two different options of materials were offered, stainless steel and a ceramic (Zirconia); they share the same dimensions, function, and operating ranges. The main difference between these two ferrules is the shape of the tip, for a non-specified reason they have a different angle that later on made an important difference when aligning the ferrule to the center of the membrane. The stainless steel ferrule has a flat tip while the ceramic ferrule has a pointy tip with an angle of 55.22°, this allowed the ceramic ferrule to go deeper into the sensor and closer to the membrane, this has a direct impact in the reflection intensity and provides better accuracy to the thin film's deflection readout.

It was decided to have both ferrules' materials tested, incorporating two couplers so there could be a comparison in performances and the importance of the tip's angle, although a modification to the stainless steel ferrule was done (polishing the tip) so it could further reach the membrane.

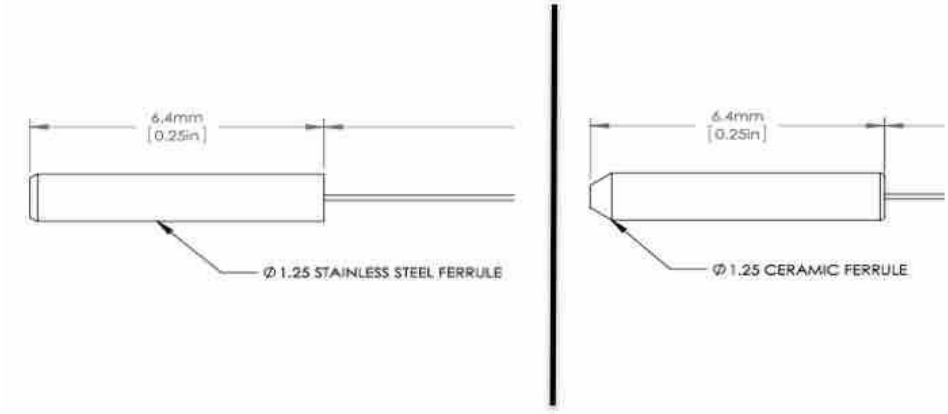

Fig. 8. Comparison of the ferrules' tips, Stainless Steel vs. Ceramic; provided by Thorlabs. Modified from [27] [28].

The fiber inside the ferrule has to be polished. While performing experiments with the fiber inside the ferrule, every time the tip touches any surface (the mirror or the membrane, for the case of this type of device) it has to be re-polished to get rid of scratches that easily affect the performance of the device. Unlike the connectors, the ferrules do not have a plastic tool to offer support and guidance during the polishing steps, consequently, the ferrule has to be thoroughly gripped and maintaining a parallel position with the polish film, repeat the previously described movements.

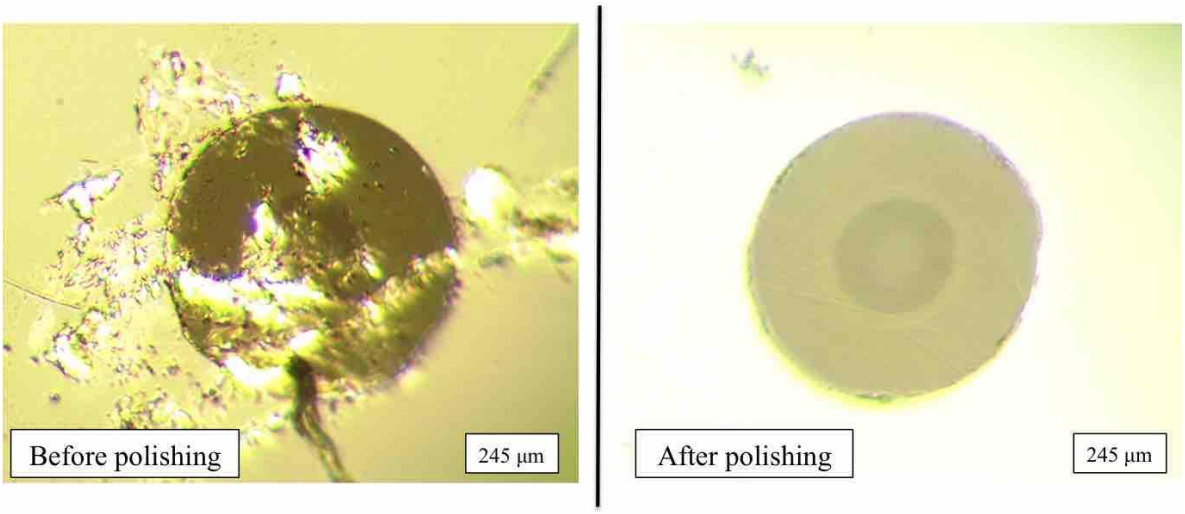

Fig. 9. Comparison of the fiber's tip inside the ceramic ferrule, before and after being polished.

The light from the source is launched from the source (LED) into the input fiber of the coupler and propagates along the lead in / out fiber end, after the loss the light suffers at the first border, the end face of the output / input fiber (around 4%) [19], that is in contact with the air cavity and will receive the reflected beam. The smoother the polishing job is performed, the less amount of loss (extra to that 4%) the light will suffer when exiting the fiber and entering back to it.

4.2.4. OPTICAL COUPLER

To achieve the carriage of information that light transports inside the fiber, an array of 50:50 splitting ratio coupler is required, it is composed of two input legs and one output leg that can be utilized for different applications, such as analysis of two beams of light that can superimposed (having constructive interference), or to analyze the interaction of a clash of signals (destructive interference).

The experiments require a quality coupler where the performance of both input legs is close the being identic; later on, the experimentation showed very little variation when switching these two legs to receive light and deliver a signal for the photo detector to interpret, it is also bidirectional and this allowed to test it, in case it had being damaged during the experiments (by shining a common light at the input or output legs and seeing it exiting the other leg).

Different options were considered, mainly comparing the specifications of the couplers such as wavelength range, pricing, reflectance and approximated loss after being connectorized from the tips. The FCMM50-50A from Thorlabs with 1x2 Graded-index multimode fiber optics coupler is selected, mainly because apart from providing the mentioned requirements, it also has a protective jacket for

the fiber that gives extra security while testing it; one more advantage of selecting this supplier is that the coupler could be customized so that the ferrule (that was also purchased from Thorlabs) was attached from fabrication and this way we could get rid of the connection (and connectors) between the coupler and ferrule, saving losses and scattering of light.

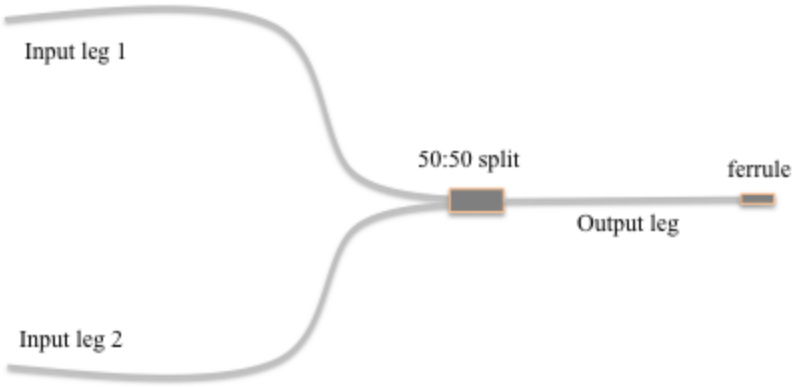

Fig. 10. Schematic of the coupler, with a 50:50 splitting ratio.

The FCMM50-50A coupler that was used to split the light already had the ferrule attached to the tip of the output fiber, but required SMA connectors for the input legs, that are hooked up to the OSI.

The process to attach the connectors requires the peeling of the fiber using a fiber-stripping tool, removing the protective jacket up until around 2 cm from the tip, this way, the remaining jacket functions as a blockage when inserting it into the connector. The fiber has to be dip into an epoxy mix, consistent of a kit with two different resins; when combined in a micropipette and stirred, a resultant viscous hardener epoxy is what allows the fiber to be attached to the inner of the SMA connector. A large drop of epoxy is caught at the tip, immediately proceed to inset the fiber with the droplet inside the connector and push it until the jacket reaches the barrier. The epoxy cures with temperature hardening inside the connector, while resting on top of a hot plate that was preheated to 100° C, the connectors were left on top of the hot plate for 1 hour, until the epoxy cures.

Fig. 11. Image of the input legs of 2 couplers with epoxy curing on top of the hot plate at 100° C. Some connectors still have the tip of the fiber that was later cut for polishing.

Once the resin cures and holds the fiber in a fix position inside the SMA connector, the remaining fiber outside is cut leaving a flat cleave that has to be polished so that the light exits the fiber with no angle and no constrains due to scratches or debris. In order to have a favourable polished fiber tip, we use 4 different hand polish films (Aluminum Oxide and Silicon Carbide) in successive steps with decreasing size grit that provides a finer finish.

The polish films and the size grits that were used are (in order): (1) 5 μm – black film, (2) 3 μm – red film, (3) 1 μm – green film, (4) 0.3 μm – white film.

We use the connector with each film with the aid of a plastic gripper that holds the stainless steel piece in a 90° to achieve flat cleave at the fiber's tip. We proceed to make smooth but precise movements simulating a ∞ shape. When switching from a rougher film to a smother one, the fiber is cleaned with Isopropyl alcohol to eliminate residual contamination.

Figure 12 shows a comparison of a damaged fiber tip inside the connector, as a result of experimentation.

Fig. 12. Comparison of the tip of the fiber inside a connector before and after polishing.

The fibers inside the connectors must be protected when are not being used, with plastic covers that avoid dirtying the tip, where the core and cladding are exposed.

If the tip of either connector would suffer accidental scratching, or damage due to the testing of the device, or contamination accountable to the environment (which could later on be noticed with a decrease in the intensity of the signal), both tips were taken for revision under the microscope and possible re-polishing and cleanse with Isopropyl alcohol.

4.2.5. OPTICAL SENSOR INTERROGATOR (OSI)

A signal acquisition system was designed at the SIMSlab with the main purpose of avoiding and substituting the use of a spectrometer that would increase the price of optical interferometers and make them unsuitable for commercial use.

The OSI works with the same principle: provides and receives light that can later on be broken into its spectral components, analyzing fringes and converting the photons into electrons which are digitized as a function of the wavelength and read out via a USB port into a host computer. The OSI consists of a circuit that enables communication with a microcontroller (Arduino Nano) that takes care of the processing of the signal. The Arduino implements a gain scheme (PGA Gain Selector), which can be re-programed based on the specific needs of the application. Alongside, a Sample Rate Selection (SR) can be established as well to set the period in which every reading will be taken.

4.3. SYSTEM ASSEMBLY

The traditional configuration of a FPI is illustrated in figure 13. The system includes a light source (LED, 850 nm) that shines multiple beams of light through a coupler made with a multimode fiber that splits the light with a 50:50 ratio, at the end of the output / input tip of the fiber, there is a protective ferrule that holds the fiber in position inside the pressure sensor. The ferrule is attached to the pressure sensor after aligning the core of the fiber to the center of the deflective membrane.

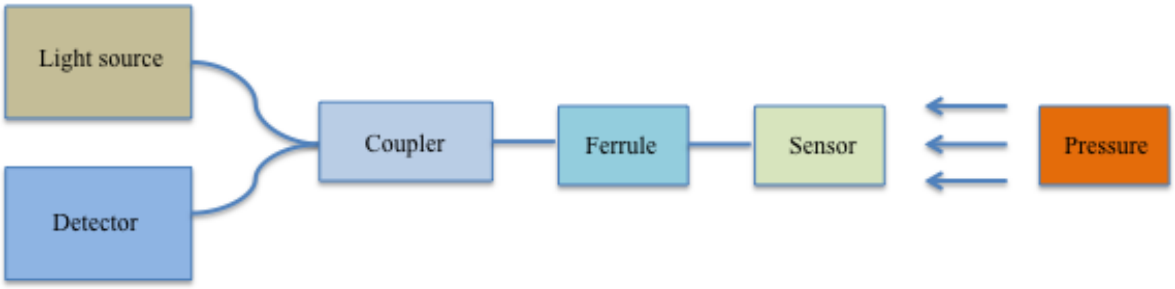

Fig. 13. Optical pressure sensor configuration.

A low finesse Fabry – Perot cavity is formed between the tip of the fiber and the thin film, in which multiple beams will be reflected creating constructive and destructive interference between them.

The result of this interference will create a change in the intensity of the light that gets reflected back into the fiber; the intensity will be altered by changing the distance of the FP cavity, which happens every time pressure is applied on top of the Silicon membrane.

The remainder of the light propagates back into the fiber, to the other side of the split, which has a photo detector in the end. The photo detector receives the resulting beam and converts its spectral components into a digital signal that later on is analyzed by the microcontroller inside the OSI.

The interaction between these reflected beams will result in a change of intensity of the initial laser beam incident on the input mirror surface (in the case of this device, the silicon membrane) [29].

The interference between the light that comes out of the fiber and back to it can be described by:

$$I = 2I_S(\lambda)[1 + \zeta\cos(\phi)]$$

Where:

- $I_S(\lambda)$ is the intensity distribution of the light source
- ζ is the fringe visibility of the Fabry-Perot Interferometer (FPI)
- ϕ is the round-trip phase shift

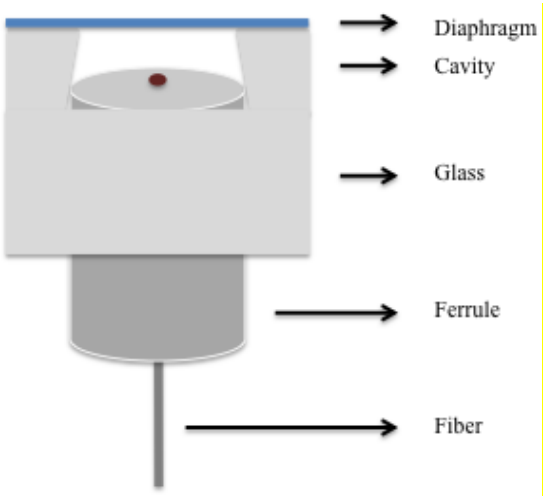

Fig. 14. Optical pressure sensor components.

Figure 14 shows a close up to the parts that form the Fabry – Perot resonator in addition to the pressure sensor consistent of the silicon diaphragm. The ferrule that holds the fiber is attached to the inside of the glass wafer below the thin film and the FP cavity is the distance between the fiber's tip and the bottom side of the membrane.

The assembling of the device was done following the next steps:

- Prepare the stainless steel cap with double sided tape to attach the sensor once it is aligned to the ferrule; place the double sided tape in the opening of the cap and cut the area that covers the opening so that it remains uncovered and the membrane can be directly hit by the stimulus of pressure.
- Put the ferrule inside the housing (protective housing that MorHeat solicited and provided, a stainless steel threaded pipe fitting, ½ male x ¼ female) taking advantage of the tight fight that was designed to hold the position of the ferrule, as shown in Figure 15.
- Once the ferrule is secured, place a drilled sensor on top of the ferrule that holds the fiber inside; simultaneously, have the OSI on so that a reflection signal can be read and it can be known when normal incidence is achieved, based on previous testing, the top value of reflection is known (~ 12 mV).

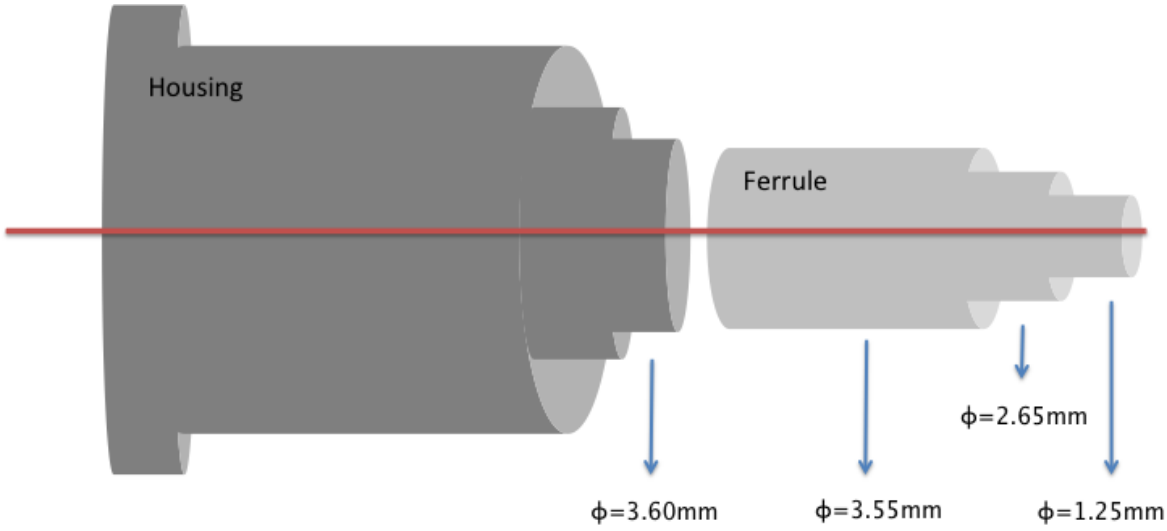

Fig. 15. Schematic of the tight fit that was used to position the ferrule inside the housing.

- When achieving normal incidence, place the cap that contains the double-sided tape on top of the sensor, so that when it closes with the housing, the opening on the cap will be aligned with the center of the sensor that contains the deflective membrane. The double-sided tape will keep the sensor in place with regards to the cap; at this point the cap and the housing may be separated to properly (semi-permanently) attach the sensor and the cap, with the use of an epoxy.
- Different types of epoxy mixes were tried to save space while maintaining adhesive force in the boning of the sensor:
    - Elmer's (Silicone Rubber Sealant):
    - Epoxy technology (Epo – Tek)
    - Loctite – Adhesive (UV epoxy)

Using the Loctite adhesive for its superior endurance with higher pressure ranges while occupying less space inside the cap was one of the tested methods, but the curing method that requires a specific UV wavelength plus a high intensity of the UV lamp (not available within the university space and expensive to purchase) led to a curing job that did not suffice to harden the epoxy entirely, a set of 3 trails was planned to test the device with this epoxy but the adhesive did not withhold the pressure and the leaks pushed the ferrule back, which led to a failure in the experiment.

Ultimately, the same Epoxy mix that was used to attach the fibers to the connectors was the one selected to seal the sensor to the cap and the cap to the housing (Epo – Tek).

The curing time for the epoxy mix (left at room temperature) is 24 hours.

4.4. REFLECTION TRIALS

Confirmation trials were carried out to test the device's functional status before permanently attaching the device (using Epoxy to fix the materials); a simulated environment was put together to recreate the conditions in which the FPI would perform.

For this purpose, a list of the following materials was adapted:

- Micro-adjustable Platform XY: To have an accurate control of the changes in distance (simulating the deflection of the membrane), it provided repeatability in positions and robustness to the setup.
- Mirror: As a reflecting surface, the first tests were performed with reflection off of a highly reflective material to ease the optimization and positioning of the ferrule; later on the reflecting material was switched to the pressure sensor.
- Coupler (including fiber and ceramic ferrule): The couplers were alternated between the one with the ceramic ferrule and the one with the stainless steel ferrule, until the problem of the shape of tip arose and the ceramic ferrule was the more convenient option to work with.
- OSI: LED (850 nm) and photo-detector in combination with the Arduino program and an established gain factor of 3 (which toped the reflection intensity converted to mili-Volts to 12 mV).
- Gripper tool "Quick grip": This apparatus provided stability to the mirror, as it gave a completely static position with no play.
- Precision lapping screw: With low height and good stability, the micro-adjustable platform was mounted and screwed to eliminate external movement and lower the noise of the experiment.
- Set square ruler: To ensure that the mirror was set to a 90° angle.

The main objective of this test was to corroborate that the LED would shine a light at a specific selected wavelength (850nm) through the fiber, it would be split by the coupler, then shone to a reflective surface (a mirror) and travelled back to the fiber's tip protected by the ferrule, then to the

detector and read by the OSI circuit that sends the data to a host computer, stores it and processes it through a LabView program.

The concept of a Fabry Perot Etalon declares that the shorter the cavity distance, the higher the intensity of the reflection; thus, this trial consisted on moving the mirror surface closer to the fiber's tip so a change in reflection could be appreciated.

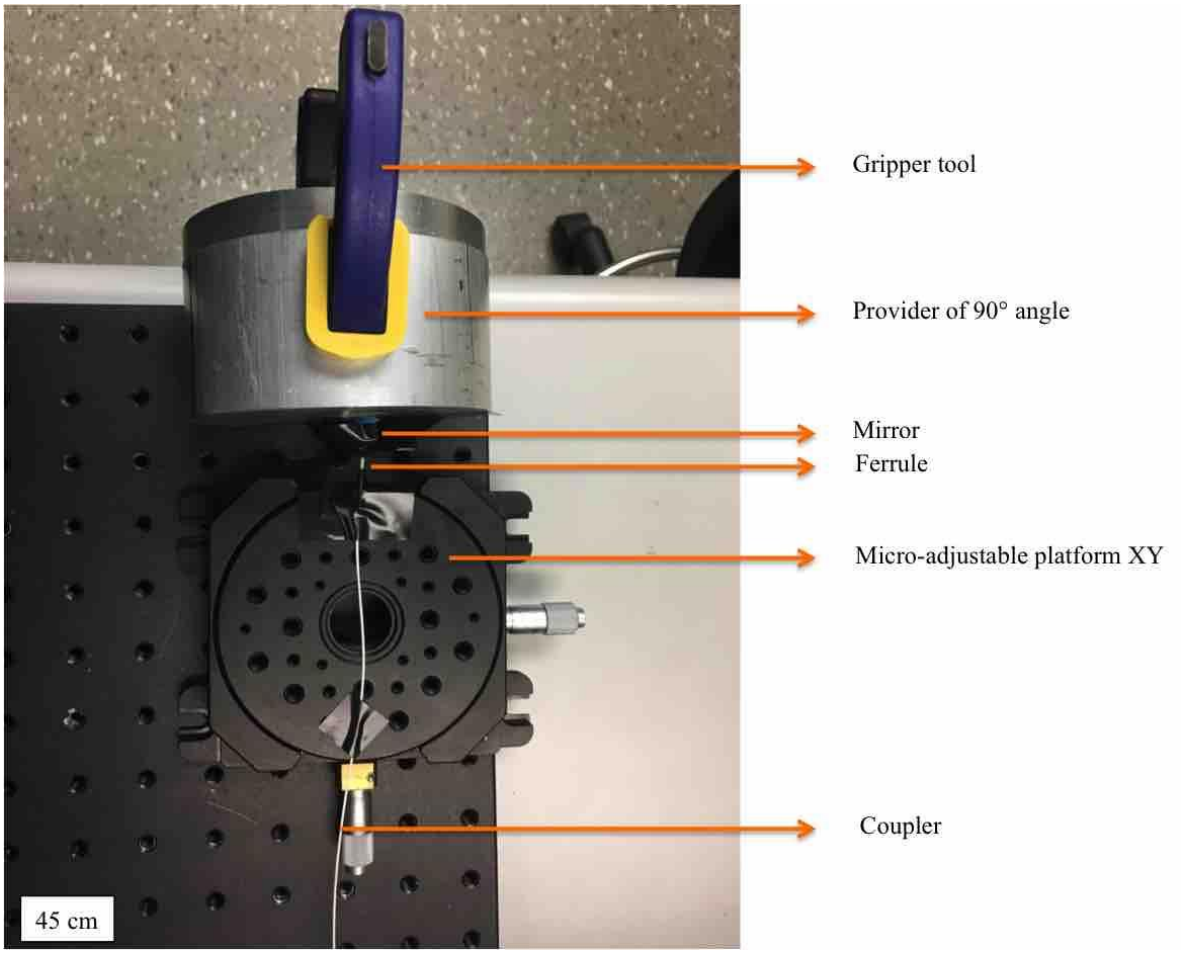

Fig. 16. Setup used to test reflection of light with a mirror surface.

The set up that was assembled in Figure 16, was meant to test how the reflection of the light behaves when simulating a variation in cavity distance, this shows a change in the intensity of the signal (mV), created by the separation of the two surfaces involved in the FP system (the mirror and the fiber). Note that a perfect mirror has a highly reflective surface (with a refractive index of 0), and has no transmission or absorption of light, domestic mirrors are not perfect as they can absorb a portion of

the light they receive, they have a coating of either silver or aluminum in most cases. For this project, a mirror from Ocean Optics was used for the sensor's tests, the WS-1 which is a diffusion mirror made from PTFE (PolyTetraFluoroEthylene) and is > 98% reflective in a wavelength range that goes from 250 – 1500 nm.

The incident beam was adjusted experimentally by sensing the output response in mV and testing the factors that interfere with the intensity.

4.5. CAVITY DISTANCE

The procedure to experimentally determine the cavity distance can be performed with aid of the setup shown in Figure 16. The micro-adjustable platform allows the control of the movement and displacement of the ferrule with regards to the thin film; horizontal modification of the distance between the two reflecting surfaces was done so a study of intensity of reflection that can be associated with distance variation could be performed.

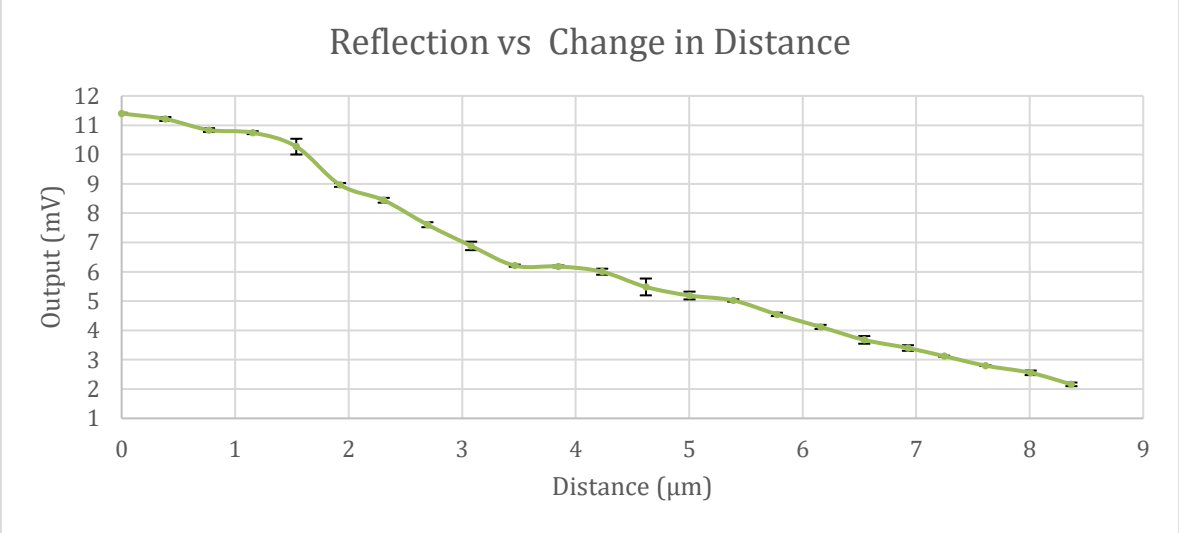

Fig. 17. Plot of the average of the first set of tests of reflection using the silicon membrane of the pressure sensor.

Figure 17 shows the average of a set of 3 trials where the complete environment of the sensor was simulated, including all the materials that would later take part of the device.

Whilst the sensor showed a linear tendency in response to the change in cavity distance, the standard deviation shown is accounted to such an alignment-dependent sensor; any minor offset between the tip of the fiber and the center of the membrane would throw an in-precise reading. However this test allowed verifying the intensity converted to mili-Volts that the device shows when having a change

of distance between the two reflecting surfaces – which could later on be directly applied to set the cavity distance at 12 microns.

4.6. EPOXY MALFUNCTION

The importance of the application of epoxy inside the stainless steel cap to secure the sensor and align it with regards to the ferrule was tested with different amounts of sealant.

Once that it was decided to work with Epoxy technology (Epo – Tek), various tests for performance vs. amount of sealant were performed. The amount of sealant to be used inside the cap to properly hold the sensor with no pressure leaks was unknown. The main condition to be considered was that there was limited space inside the cap once the sensor is set in place; if too much epoxy is used, the cap can not properly sit on top of the housing, this creates a condition of miss-alignment and directly affects the reflectivity of the sensor. Normal incidence is a necessary condition for the FPI to have constructive interference that is translated to full I_R (Intensity).

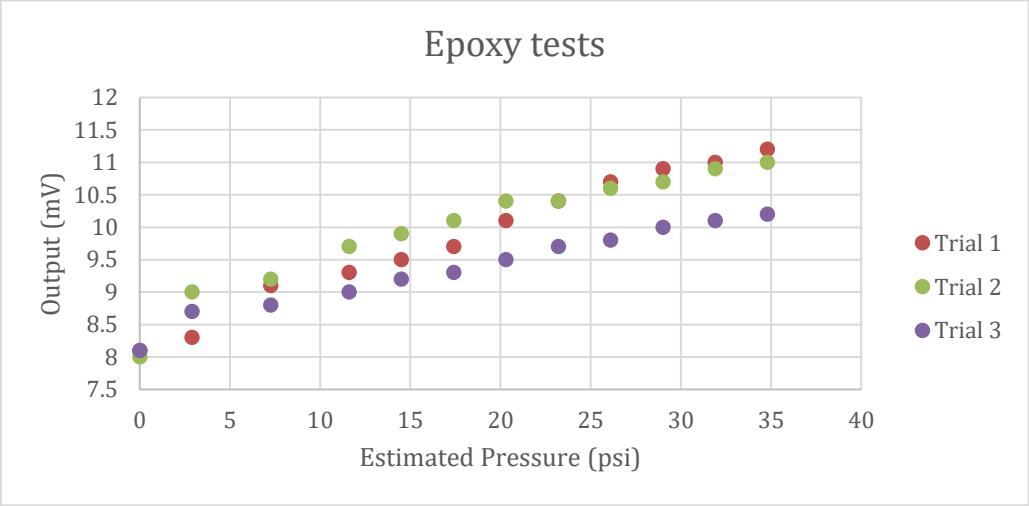

Fig. 18. Set of tests with application of excessive amount of epoxy inside the stainless steel cap.

Figure 18 shows a set of tests that was performed with an excessive amount of epoxy inside the cap, to secure the sensor in place. These tests arose from the uncertainty in the volume of drops used within the cap. The measurement of the sealant was done in drops, with an average needle ranging in 1 mL per 20 drops, therefore ~ 1mL of epoxy was applied in the first instances of the experiments.

As seen in figure 19, the situation that was created with this amount of epoxy was that there was an overload of sealant inside the cap; when it hardened, the epoxy level was ~ 1.3 mm. The distance that

the inner diameter of the housing has to place and sit the cap was 2mm, so as the cap was full of sealant, it could not be properly placed and closed. Additionally, the epoxy has a give when pushed or compressed to a certain extent, this caused a play and variation in the results of the experiments in figure 18.

The variation of the output in mili-Volts happens due to the compression that the epoxy suffers when it is pushed from the effects of pressure, moving the sensor from a fixed position and altering the reflection (R), therefore, the intensity. This set of tests was done with the complete assembled sensor inside the pressure chamber, to simulate the real conditions in which the characteristics of the sensors were studied.

To correct this condition, less amount of epoxy is used to secure the sensor. An experimental test was done with 4 drops and another one with 8 drops.

Having less drops of epoxy inside the cap, reduced the previously occupied space, allowing for a proper sitting of the cap on top of the housing; once this condition was no longer a problem, normal incidence was achieved between the fiber and the silicon diaphragm, which is translated into more constructive interference of the beams inside the FP cavity.

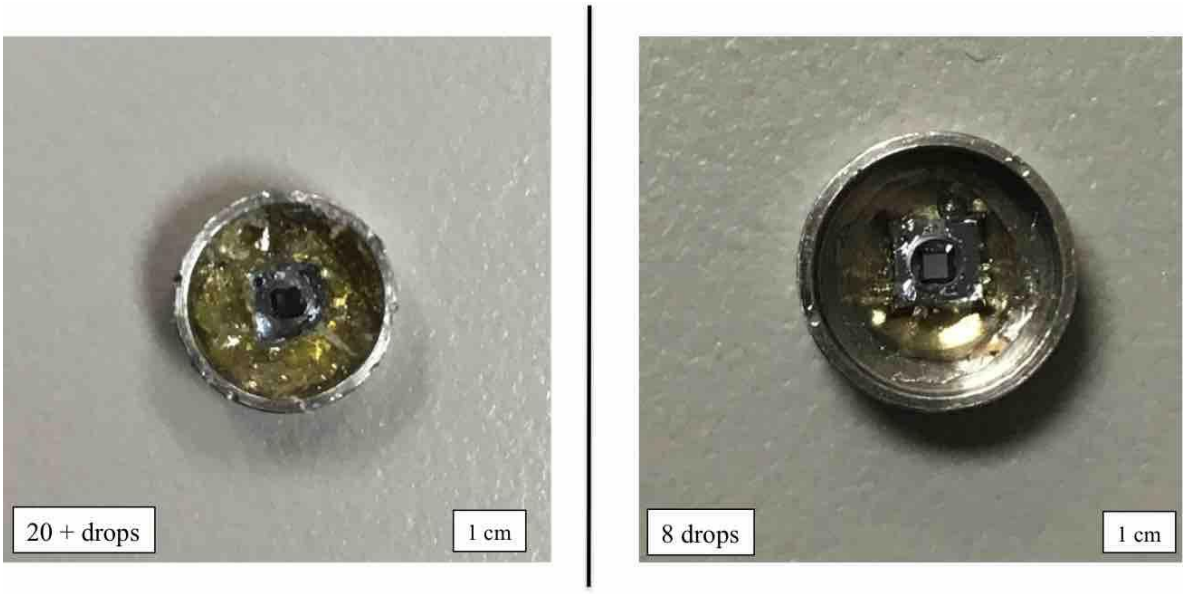

Fig. 19. Comparison of the pressure sensor inside the cap with variation of the amount of epoxy drops used for attachment.

The curing method for this epoxy, as previously explained in section 4.4, consisted in placing the cap once the sealant was applied, on top of a hot plate at 100 °C. Approximately 1 hour is required for the epoxy to harden.

4.7. PRESSURE LEAKS

While testing the device inside the pressure chamber, one of the conditions that surged was the pressure leak inside the protective housing of the optical pressure sensor. The majority of these leaks came from openings or bubbles of air between the epoxy and the sensor, due to a bad technique when applying the sealant; the possibility of compression and therefore, leaks or air, pushed the sensor from the surface of the cap or moved it from the fixed position that was previously set.

This condition led to practice and correct the epoxy application quantity and technique, as the miss-alignment of the sensor and the ferrule are notoriously detected based on the response of the intensity of reflection.

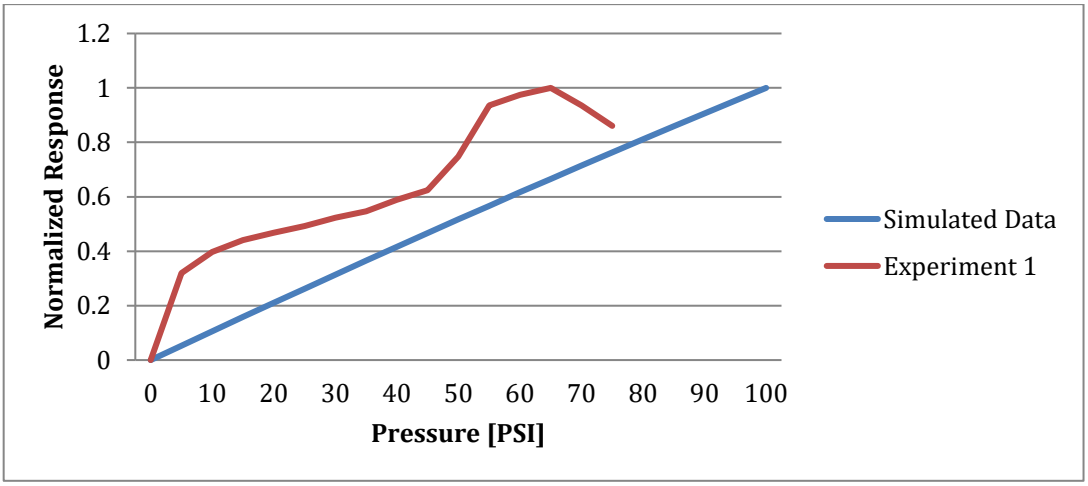

Fig. 20. Set of tests of reflection with a failed technique of epoxy application.

Figure 21 depicts the response of the fully assembled sensor inside the pressure chamber.

The sealant had leaks occasioned by a failed application technique and amount of epoxy; the test showed a discrepancy with the simulated slope since the first levels of exposure to pressure, pushing the membrane back until it totally snapped after passing 70 psi.

The experimental results shown in figure 20 follow the same trend as the simulated slope, however there is an offset that goes from 5 – 45 %, with increases and decreases that are accounted to the unwanted movements of the sensor.

Chapter 5

Sensor performance and final results

In this chapter, the results from experiments described in the previous chapter are presented, post-processing is performed and a comparison between the theoretical analysis and the experimental results of the FP optical pressure sensor is done.

Once the setup was properly assembled and calibrated, several experiments were carried out to further study the behaviour of the device, the response was normalized and in tune with the simulated data; finally, a characterization is presented, including features such as sensitivity, accuracy and linearity.

5.1. FINAL ASSEMBLY

The final optical pressure sensor is presented in figure 21, it is adapted inside the housing provided by MorHeat ©; a stainless steel threaded pipe fitting, ½ male x ¼ female which is screwed into the pressure chamber, previously covered with a layer of Teflon tape to eliminate air leaks.

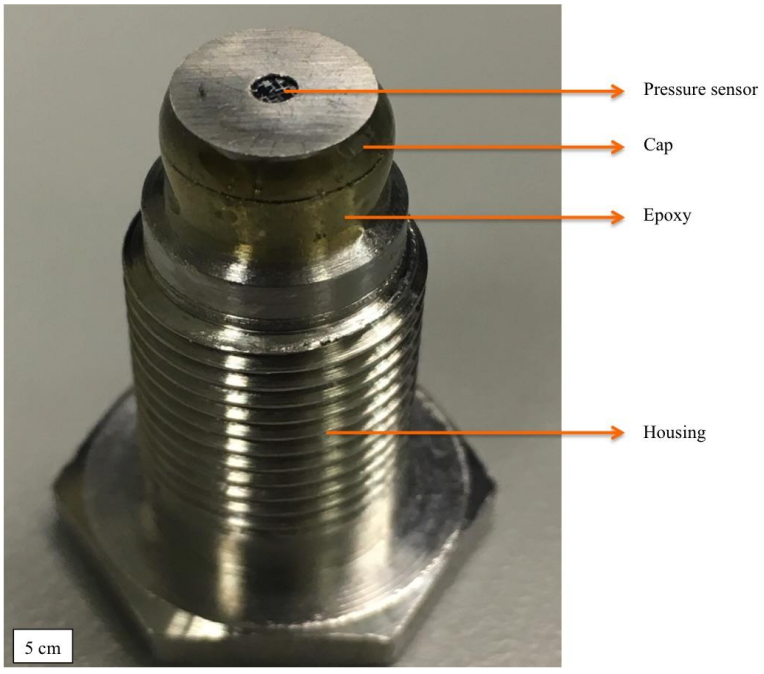

Fig. 21. Optical pressure sensor assembled.

The stainless steel cap with the pressure sensor inside, was positioned on top of the housing and attached with the same epoxy mix that was used to fix the sensor inside the cap, a thin layer of sealant was applied to the junction between them and sprayed evenly to facilitate curing, the layer is ~ 0.5 mm thick. A variation in the response of the sensor was detected when resting the cap on top of the housing without an uneven spraying of epoxy to seal the junction, the correlation between the normal incidence of the light and the intensity of the reflection is linear and it was through the previous experimental setup testing that a standard level of intensity was set, so it was known whether the sensor was performing correctly or something needed to be corrected.

The experimental setup, the assembling and calibration as well as the testing, were performed at the SimsLab, the complete apparatus allowed characterization of the device at room temperature (25 °C), starting from atmospheric pressure up to 95 psi.

The pressure can be monitored at two stages; an analogic gauge which is directly attached to the airflow that comes from a pipeline and a digital gauge with a plastic case, 2-½ dial with ¼ bottom connection, manufactured by ABS ©.

During the testing, the device was exposed to constant rises and decreases of pressure; it was important to confirm that the sensor's response is equal when increasing and decreasing the pressure applied, so that a specific amount of pressure was always associated to the response of the intensity, with no regards of the membrane deflecting or coming back to a flat position. The sensor demonstrated no noticeable variation to the ups and downs in the amount of stress that changed the position of the membrane.

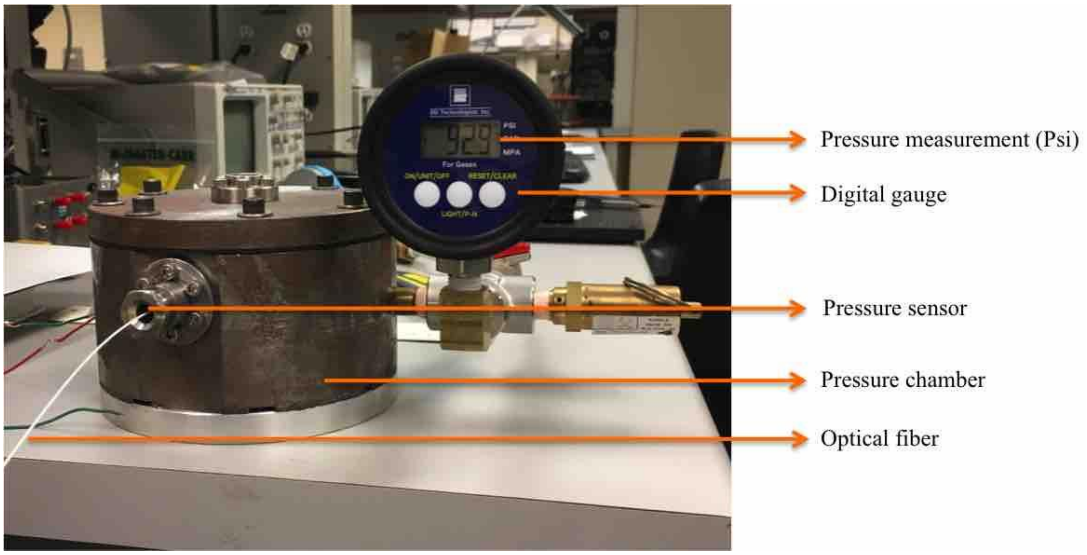

Fig. 22. Test setup for pressure measurements.

Figure 22 shows the pressure chamber with the optical pressure sensor inside and the optical fibre that sticks on the back of the stainless steel housing, during a highly elevated pressure run.

When the pressure level surpasses 96 psi, the pressure chamber's safety relief valve actuates and lets the air flow escape throw the side of the chamber.

The silicon membrane was directly exposed to the airflow and all the measurements were recorded in real time. The response time of the thin film is reported to be less than a second, but the time it took for the optical pressure sensor to stabilize at each different level of pressure when tests were being done, depended on the calibration of the diaphragm with regards to the tip of the fiber.

An estimated time of 2 seconds in average was set before recording the output response (mV) given by the device at any given pressure. The response of the light is competent enough for a device whose applications are aimed to the industry; the membrane needs an average of 1 second to receive a change in pressure that is detected by the optical system. There are available approaches to accelerate this response time, the most effective being increasing the reflectivity of the mirror-like surfaces that form the FP cavity; however, this device was restricted by the capability of the electronics, which is outside of the scope of the work presented in this thesis.

During the testing of the sensor's response, larger sessions of trials were performed to see that the detected pressure at a specific moment could be held by the device (later converted to mV), these trials consisted of exposing the membrane to a certain amount of air flow (30, 40, 50 psi…) and get an output response, which was left running for extended periods of time (5 – 10 minutes); the output response had a variation of +/- 0.01 mV on average, which represents less than 1 psi. This was the error found accounted to the sensitivity of the circuit.

5.2. EXPERIMENTAL LOSSES OF THE INTENSITY OF LIGHT

Besides the theoretical factors for loss of intensity that are characteristics of the FP interferometer, we find external agents that contribute to the loss of power of reflection.

The incident angle of the light plays a crucial role in the factual performance of the light path, if the light does not have normal incidence, then the loss factor (V) is augmented due to scattering. Accordingly, guaranteeing that the mirror was in fact set parallel to the fiber is a necessity.

Another external factor that directly affects the signal is the bending or micro-bending of the fiber, which can be defined as accidental bending of the coupler that may occur while handling the materials involved in the experiment, any tight bends would contribute to the increase in the loss factor (V).

Assembling factors that can affect the experiment are:

- Connections of the input legs to the OSI: Every time the coupler was disconnected from the OSI and re-connected, the system had to be verified with a basic reflection test to confirm that the light was in fact entering and exiting as it was intended.
- Cleanliness of the mirror: The reflective surface, in this case the mirror – later on, the membrane had to be properly cleansed to get rid of any potential dust particles, debris and contamination from the environment, as these particles would directly affect the light path, thus, the intensity of reflection.
- Polishing of the fiber's tip: This step turned out to be of major importance in the first experiments; in the process of calibration of the fiber in regard to the reflecting surface, unwanted scratching occurred at the ferrule holding the fiber inside, this micro-scratches were obstructing the light path and were reckoned to be the cause of the lessened intensity.

The silicon membrane has a much higher index of refraction ($n_S = 3.2$) than the mirror ($n_M = \sim 0.04$), which means that absorbs more light than the mirror does, for this reason, the theoretical analysis showed that the loss factor (V) would increase and less intensity (later converted to mV) was expected. Nonetheless, the previously learnt insights helped in the optimization of the setup and alignment of the fiber's tip in regard to the center of the membrane, which is where the deflection achieves the highest point.

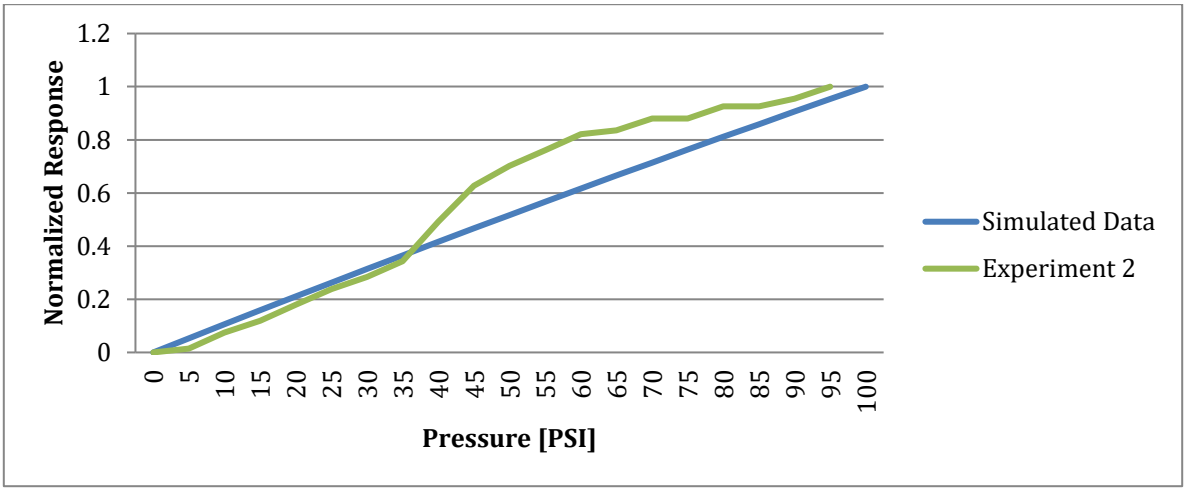

Fig. 23. Average of the initial experiments with the optical sensor.

As exposed on Figure 23, the initial experiments carried out showed the same trend as the simulated data, with a linear response of the sensor up until 40 psi of pressure applied on top of the membrane; after that, an offset of 10% is displayed with a top peak of 20% at 60 psi which later on falls back in

line with the simulated response after passing 80 psi and continues perpendicular to it up until after 95 psi.

The previous response of the sensor was accounted to the position of the sensor with regards to the opening of the cap; the membrane was not entirely centered and aligned to the aperture on the top of the structure, a condition that had to be corrected at the assembling stage.

5.3. LIMITATIONS

The main limitations found with the performance of this sensor are divided in three categories: assembly, sealant failures and elevated temperature.

The assembly process and configuration are designed in such a way that the variation of pressure will not have an influence on the sensor's alignment. However, there is no evidence that the device will have a linear response or accuracy beyond 100 psi. This is accounted to the lack of experiments conducted this range of pressure.

Regarding the epoxy, glues and sealants that were used during the different steps of sub – assembly, calibration, final assembly and tests - there is potential room of wear and breakage of the connections if the sensor is tested at higher pressure ranges. Using higher-pressure ranges for testing was not a condition added in the experimentation phase, as there is no evidence that supports the use of the joint epoxy for higher pressure ranges.

The final device was only tested at room temperature, as there is no thermometer present in the design. There was no thermal – change considered during the development of the sensor and this is an important limitation in the study of a device aimed for harsh environments.

The materials that are involved in the body of the pressure sensor are reported to withstand up to 85 °C with no alteration to their performance. Nonetheless, further study and implementation of a thermal response of the materials is necessary to assess this limitation. An isolation system can be used to prevent the heat transfer suffered from the protective housing into the sensing and transmission elements. This device has no isolation as all the parts are connected or in close contact with the main body of the sensor.

5.4. SENSOR CHARACTERIZATION

A simulation of the device's respond was chosen so a comparison could be made with the ideal response of a FP resonator with the characteristics of the sensor presented in this thesis. To determine

the transmission and absorption of the device, as well as the frequency for the wavelength to complete a whole sinusoidal cycle, a linear base model with normalized data was selected.

Each of the measurements that was taken for the following characterization include a previous validation of the correct positioning of the fiber inside the protective housing that was done with the output response when there is no pressure applied on top of the membrane.

Table 4 shows the parameters used in the simulation of the Fabry – Perot resonator:

Table 4. Parameters for FP simulation response.

Symbol	Parameters	Values
C_O	Speed of light	3×10^8 m.s^{-1}
η	Refractive index of air	1
η	Refractive index of glass	1.5
η	Refractive index of silicon	3.42
ϑ	Thickness cavity	5
R_1	Reflectivity of the mirror 1	3.45%
R_2	Reflectivity of the mirror 2	29.97%

The sensor was tested under the same conditions as the initial set ups, at room temperature (25 °C) with increments of 1 psi to test sensitivity and 5 psi to test endurance and stability of the membrane – fiber array.

As seen in the simulation below, the data reflects a straight forward response as expected from a FP interferometer [30]. This fundamental approach has a phase modulation to generate a stable value that correctly reflects the rise of pressure that was experimentally tested. Although the results of the experiments show a slight variation with the simulated data, the trend is in good agreement.

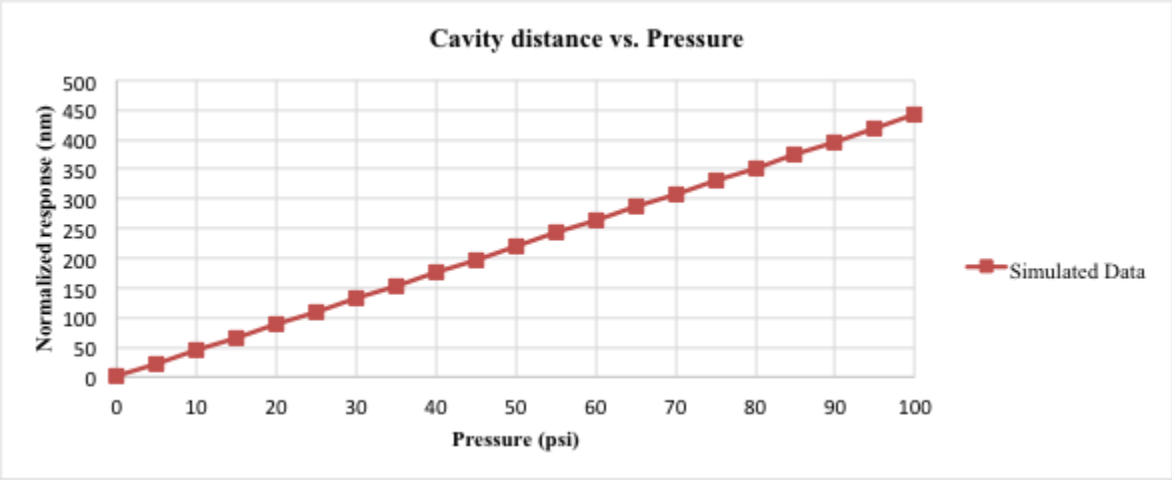

Fig. 24. Simulated response of the change in cavity distance of the FP resonator.

The simulated data shows a linear response to the change in cavity distance, the expected change of cavity length (*dL*) per unit change in pressure (*dP*) is 4.4068 nanometers as shown in Figure 23, over a range of 0 – 100 psi with steps of 5 psi. The membrane's deflection is accounted to be 1.23% of the membrane's thickness; therefore it is considered as small film deflection.

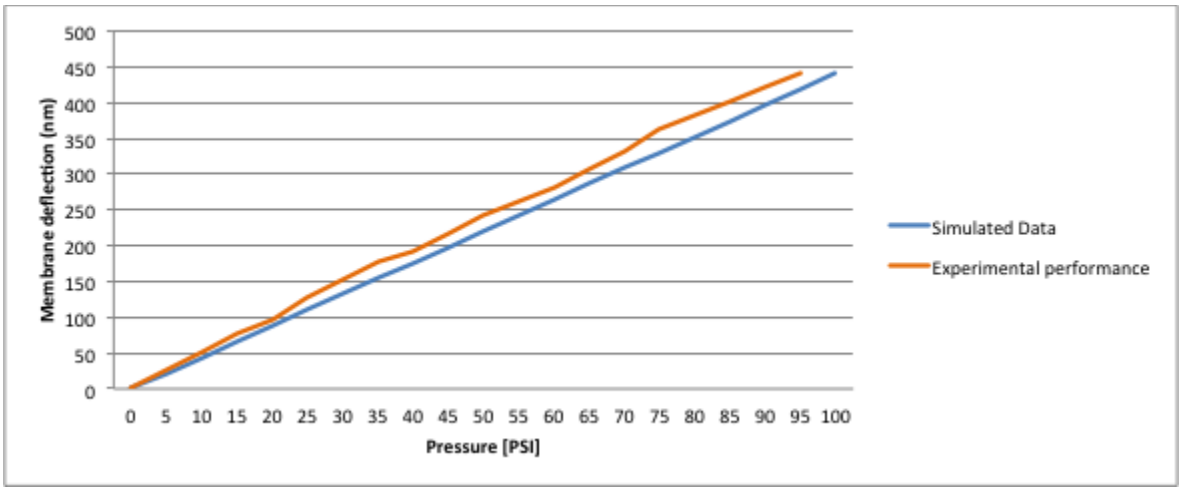

Fig. 25. Comparison of the simulated response vs. the experimental performance of the optical pressure sensor.

The experimental performance of the sensor shows an average response of *dL* per *dP of* 4.5156 nanometers. This reflects an average offset with the theoretical analysis 2.4 %, with a difference of 0.1088 nanometers per psi and in the worst case, a difference on average of 0.24 nanometers per psi. This offset is accounted to the little imperfections of the setup assembling and the possibility of miss-alignment with the exact center of the membrane, where the most amount of deflection occurs. The response time taken for each lecture is 2 seconds. During the testing of the sample, each sample of

the graph shown in figure 25 was taken once the pressure stabilizes to the upcoming rise of pressure. The sensor shows stability to the stimulus of pressure once the air leaks were corrected.

5.5. ACCURACY

The accuracy of the FPI is defined as the difference between the actual optical value of the intensity reflected from the system and the measured value of the device. Although the accuracy is affected by different factors such as the total internal reflection, the angle of incidence of the light and the intensity, it is mostly dependant on the instrumentation that is used to acquire and process the signal. In the case of this setup, the circuit that was utilized to demodulate the intensity of the light, is what gives the accuracy to the readings.

The membrane itself has a reported accuracy of 0.1 psi, but due to the electrical system + the Arduino program that are used to convert the light into mili-Volts, the FPI setup (involving the silicon membrane as one reflecting surface and the silica fiber as the second reflecting surface) can only detect as low as 1.25 psi.

A set of 3 trials of experiments was carried out to test the accuracy of the device; same that is dictated, as previously mentioned, by the circuit. The steps that were taken during the experiments consisted of 5 psi at a time; the research done with these sorts of devices (aimed for automotive, plastic, aerospace, manufacturing) has an average accuracy of 40 – 50 psi, which gave the value selected for each step in this study. Ultimately, the accuracy would be increased by a factor of 10X.

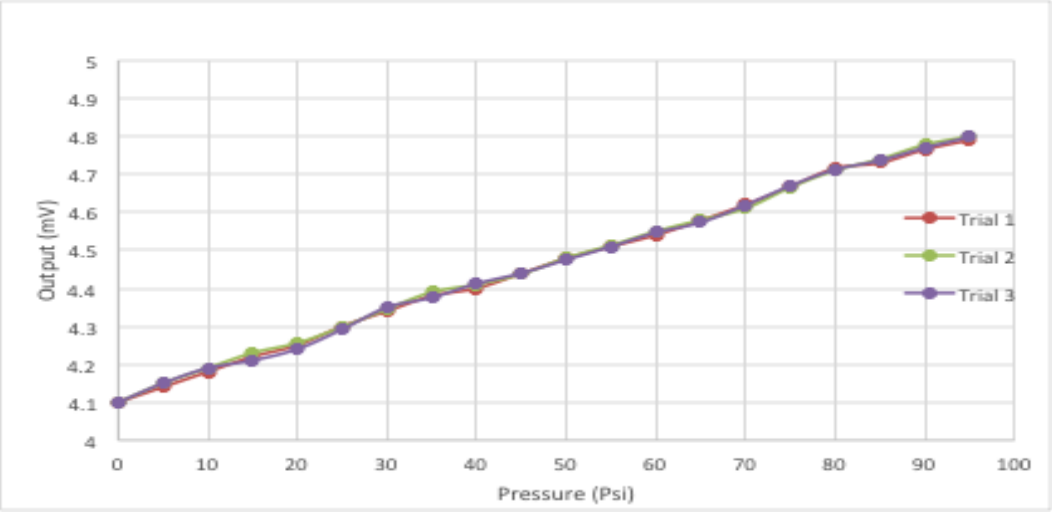

Fig. 26. Pressure sensor's response to accuracy tests.

Figure 26 shows the result of the experimental study that was performed to test the accuracy of the device. The procedure was done by repeating the stress stimulus on top of the membrane in order to acquire a specific amount of intensity of reflection, which can be readout as the output in mV. As it can be seen with the data collected, the setup shows a linear and close response with different trials, and this can be translated to a good repeatability and stability of the sensor.

However, as mentioned before, the accuracy can only go as low as 1.25 psi due to the circuit's characteristics. If we compare this accuracy with devices like the ones reported in the literature review which are constructed alike and work on the same principle, this device would not be on the top of the list; nonetheless, it shows a good behaviour when comparing it to the traditional available technology for harsh environment sensing and that is where this device is looking for to contribute, with future work and the next prototype.

An error graph was included in this section in figure 26 to show the little standard deviation depicted in the accuracy study.

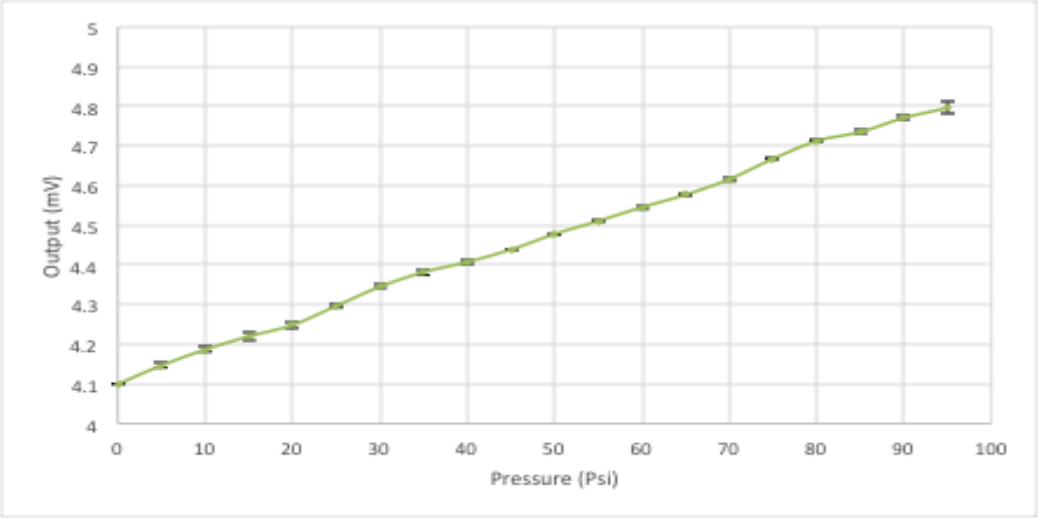

Fig. 27. Standard deviation in accuracy test.

5.6. SENSITIVITY

Sensitivity as an absolute quantity can be defined as the smallest amount of variation (absolute) that can be observed, noticed or detected by the sensing mechanism. Optical sensitivity is defined as the variation of the intensity of the reflected light per unit change (decrease or increase) in the FP cavity thickness [12].

Table 5 shows a comparison of the sensitivity reported on the sensor' specifications, the mathematical analysis and the experimental results.

Table 5. Comparison of sensitivities reported for the MEMS optical pressure sensor.

Sample	Sensitivity (mV / psi)	Sensitivity (nm / psi)	Offset
BCM sensor (spec sheet)	N/A	4.2501	N/A
Mathematical analysis	1.25	4.4068	3.55 %
Experimental results	1.3768	4.5156	5.87 %

Due to the mechanical and optical properties of the sensor, the device falls into the category of a low finesse FPI (R<90%).

The experimental sensitivity loss is nearly twice as the expected loss from the theoretical analysis and simulation. However, both (theoretical and experimental analysis) fit the optical response trend that was expected for a FPI. The discrepancy between the specification sheet and the theoretical analysis is accounted to calculations being done with approximations of the values for different properties of the material, such as Young's modulus, Poisson's ratio or the values of thickness and lengths. As for the experimental results, it is previously mentioned that alignment and calibration are key elements in the assembling of the device. Failure to reach the exact center of the membrane can cause a shift in the boundary conditions that will have an impact in experimental loss.

Optical sensitivity is affected by different characteristics of the sensor, such as mirror reflectivities, initial intensity of the beam, beam radii, cavity distance in which the interferometry will actuate. This setup and proof of concept was held with a commercial sensor which had established materials that worked as the reflecting surfaces, and given the relatively high index of refraction of the silicon, the optical sensitivity is not top range, one of the ways in which this could be improved is by sputtering a layer of gold or aluminum (around 1 nanometer thick) to the silicon and this will increase reflectance. However, due to the limited size of the whole that was drilled on the bottom of the wafer and the increased cost, it was decided to test the device without that extra metal layer taking advantage of the already good sensitivity it showed.

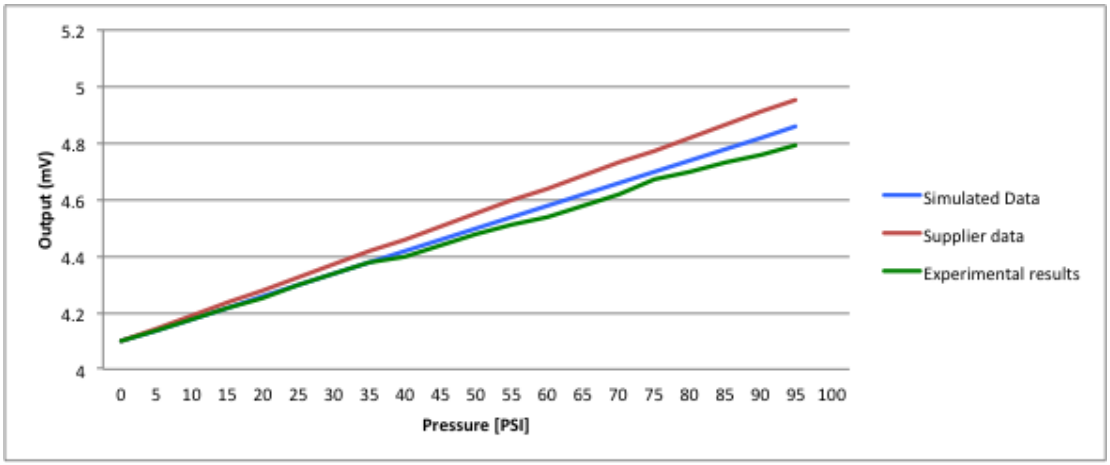

Fig. 28. Comparison between the optical pressure sensor responses. The supplier data showing the best reflectivity vs. the simulated data with a reduction in sensitivity of 3.55 %. Then the experimental results that decrease the intensity of the response in 5.87 %.

5.7. LINEARITY

Linearity, or non-linearity can be defined as the deviation of a specified graph response or calibration curve for the previously studied and established output of the pressure sensor. High-pressure linearity can be achieved by levelling the asymmetry of the FP transfer functions, by the means of highly diverging beams and the aperture of the reflected beams.

Subject to the application, certain devices require a higher level of linearity that can be increased depending on the necessity of performance. When talking about a Fabry – Perot pressure sensor, this characteristic means that whenever the pressure range over which the change in reflected intensity (I_R) is detected, has a swift, it maintains linear with the augment or decrease in pressure applied (dP). In other words, the magnitude of the reflected light inside (R) the system should be linear with the change in the pressure amplitude (p) [30].

To obtain the linearity of the system, the following expression is used:

$$A_S = \frac{dl}{\mathrm{dp}} = \frac{l}{E} \qquad (21)$$

Where,

$$dp = \frac{E dl}{2} \qquad (22)$$

- E = Young modulus
- l = FP cavity

- *dp* = change in pressure

(a) (b)

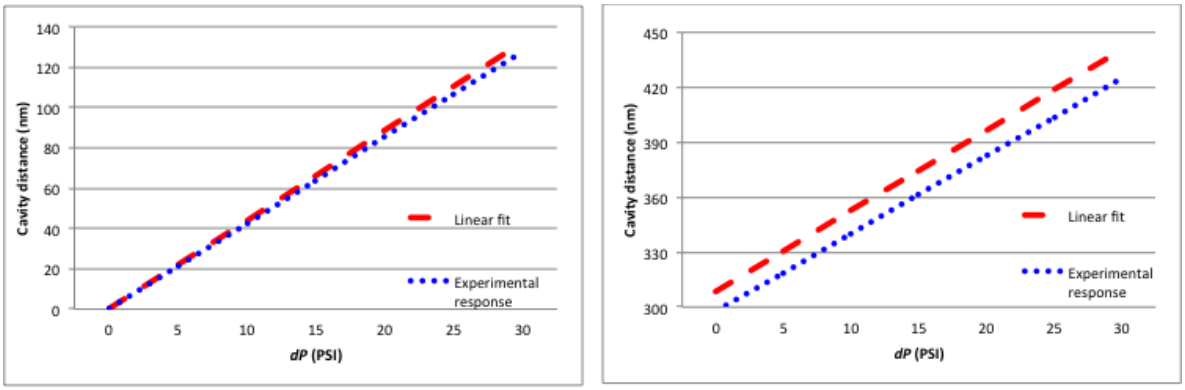

Fig. 29. Comparison of the linear fit vs. experimental response at two stages of the FP pressure sensor. (a) shows the setup's response in the first 150 nm of the FP cavity while (b) shows the non-linearity depicted at a range of 300 – 450 nm.

Figure 29 shows a linear fit to the slope of the response of the optical pressure sensor, for a pressure range of 0 – 100 psi and mirror – like reflectivities of 37 %. With a FP cavity of 12 μm and taking the displacement of the silicon membrane (*dl)* as 17 nm with a Young modulus of 150 GPa.

The formulas in this section demonstrate that the non-linearity of the system can be calculated as a useful tool to verify how the setup should theoretically behave when being assembled and tested. The maximum pressure amplitude of the experimental results, however, has a shift of approximately 0.255 with regards to the theoretical analysis; this is accounted to the little imperfections that happened when preparing the materials and attaching all the involved parts of the optical sensor. As previously mentioned, the slightest mismatch in alignment (mainly between the center of the diaphragm and the beam of light) can slightly alter the normal incidence of the light that has a direct impact in the performance of the device.

The non-linearity results are summarized in table 6.

Table 6. Non – linearity of theoretical and experimental MEMS optical pressure sensor.

Sample	Non – linearity (%)
Theoretical	0.325
Experimental	0.58

The factors that can affect the optical pressure sensor's linearity are the diaphragm's thickness, as its response in bending will have a direct impact in the intensity of reflection, as well as the indices of refraction of the mirror-like surfaces of the device; ultimately, the alignment of the fiber with regards to the thin film will also represent a major play in the linearity study, as can be seen with the mismatch between the theoretical and the experimental results.

5.8. NOISE EQUIVALENT PRESSURE (NEP) MEASUREMENT

This characteristic (NEP) is defined as the minimum detectable pressure at which the signal can be distinguishable from the noise of the environment in which the sensor is performing.

The NEP can be described as the peak to peak (averaged) noise (N), divided by the peak of the output signal (in this case, voltage) per unit of pressure (S_P):

$$NEP = \frac{N}{S_P} \qquad (23)$$

$$NEP = 0.09873$$

The NEP is directly related with the sensor's sensitivity, which in this case can be neglected as the value shown for sensitivity is not greater than the detectable NEP. Would the NEP have a lower magnitude, a filter to process the reflected beam would be a solution to increase the asymmetry of the device.

Chapter 6

Contributions, Conclusions and Future Work

6.1. Contributions

6.1.1. Improvement in the pressure range

The majority of the sensors that are reported in the literature share the traditional Fabry – Perot assembling procedure and setup. However, they withstand lower pressure ranges due to the size of the MEMS device (particularly the thickness of the membrane),, the packaging and materials used in fabrication and assembly. The functionality of an optical MEMS pressure sensor often depends on the limits of operation of the fiber or the membrane. Hence, a notable difference with this device is the aid of a protective stainless steel housing that allows the other materials to be pushed to mid-higher pressure ranges.

6.2. Future Work

6.2.1. Fabrication process

The operational ranges of this MEMS optical pressure sensor can be improved by using components that withstand higher pressure and temperature limits. Materials that present enhancement potential include silicon carbide or sapphire, recognizing each present limitations that need to be further explored.

Improvement potential also lies in fabricating the reflecting membrane via sputtering a deflective film with metal coating to increase reflectance, sensitivity, response time, and accuracy of the signal. This presents an alternative enhanced approach to the modification of a commercial sensor.

6.2.2. Assembling

The assembling and calibration for this sensor required extensive examination. The aid of additional materials was essential to support the setup and recreation of the interior operations of the FP cavity.

Some of the materials were damaged in account for the natural wear and accidental scratching of these micro components. Re-polish the fibers inside the input or output legs and cleaning the drilled sensors after exposure to contamination among the main corrections. The assembling process can be improved when fabricated components are put together, instead of doing a fit with modified materials.

6.2.3. SENSITIVITY

An optimum study of parameters is required to attain high detection sensitivity.

The relationship between increasing reflective surfaces and enhancing sensitivity is not linear. If the surfaces' reflectivities increase without a proper photo-detector and the correct beam radii, the FP interference could start diffracting inside the cavity causing a decrease in constructive interference, which means less finesse and ultimately, less sensitivity.

6.3. CONCLUSIONS

This thesis developed an optical MEMS pressure sensor capable of sensing a 20% higher-pressure range as compared to those reported in the literature.

The device was fabricated by drilling a hole through a commercial MEMS pressure sensor with a silicon thin film. This film actuates with the stimulus of pressure and deflects down as more pressure is applied on top of it. In order to eliminate electronics and complicated circuitry arrays, a Fabry – Perot interferometer was incorporated to replace the signal transmission of the device.

An FP etalon works on the principle of light reflection. Ideally, two mirror-like surfaces are placed parallel to each other with a specific distance (cavity). This length has the magnitude of the beam of light's wavelength that is being used. Constructive and destructive interference was achieved inside this cavity by shining a beam of light at 850nm.

One of the surfaces remains stationary (the fiber) while the other one (the silicon membrane) will deflect, changing the distance that separates the two surfaces. In this process, the multiple beam interference will have a shift in phase (the amount of trips one full wavelength travels along the cavity) and the intensity of the output response will vary, up and down.

The ability to alter the intensity of the beam with a change in the device's cavity distance is the result of pressure applied on top of the membrane. A photo detector, amplified by a general purpose Op – amp, in addition to a microchip with programmable gain, converts the signal to a digital readout. The

signal is then buffered, transmitted and stored over a USD drive to a host computer. This setup results in a direct relationship between the applied pressure on top of the membrane and the response in mili Volts of the LabView program used as an interface for the user. Increased applied pressure (0 – 100 psi), augments the voltage (4 – 5mV), and enables a correlation of these two values in a clear readout of pressure.

The sensor consists mainly of four parts, which are assembled and calibrated at the SimsLab: a coupler with a multimode fiber; a ceramic ferrule at the tip of the output leg of the coupler; a MEMS pressure sensor; and the protective housing. This packaging allows the sensor to be tested inside a pressure chamber while maintaining stability and accuracy of the readings.

A simulation of the response of the sensor was implemented to compare during the testing stages. The calibration (alignment of the fiber with regards to the thin film) was constantly monitored, as one of the main stages where the sensor fails. The fiber inside the ferrule was securely held within the stainless steel housing using a tight fit, in addition to a specialized fiber epoxy to seal the housing to the cap.

This sensor shows the potential to be implemented in manufacturing-like environments, however it would be a greater contribution to serve as a proof-of-concept data provider to a second prototype that can be enhanced with more resistant materials and micro-fabrication techniques.

References

[1] C. PANG, H. BAE, A. GUPTA, K. BRYDEN, and M. YU, 2013. MEMS Fabry-Perot sensor interrogated by optical system-on-a-chip for simultaneous pressure and temperature sensing. *Opt. Express*, vol. 21, no. 19, pp. 21829–21839.

[2] Y. ZHAO, C. LI, M. HAO, R. CHENG, X. FAN, and P. CHEN, 2015. Optical micro-electro-mechanical-system pressure sensor based on light intensity modulation. *IET Micro Nano Lett.*, vol. 10, no. 10, pp. 491–495.

[3] D. C. ABEYSINGHE, S. DASGUPTA, J. T. BOYD, and H. E. JACKSON, 2001. A novel MEMS pressure sensor fabricated on an optical fiber. *IEEE Photonics Technol. Lett.*, vol. 13, no. 9, pp. 993–995.

[4] F. XU *et al.*, 2012. High-sensitivity Fabry–Perot interferometric pressure sensor based on a nanothick silver diaphragm. *Opt. Lett.*, vol. 37, no. 2, pp. 133–135.

[5] H. BAE, X. M. ZHANG, H. LIU, and M. YU, 2010. Miniature surface-mountable Fabry–Perot pressure sensor constructed with a 45° angled fiber. *Opt. Lett.*, vol. 35, no. 10, pp. 1701–1703.

[6] Durham Instruments. Available: http://www.disensors.com/. [Accessed: 04-Sep-2017].

[7] Pressure Transmitter suppliers,manufacturers -Micro Sensor. Available: http://www.microsensorcorp.com/product-pressure_transmitter.htm. [Accessed: 04-Sep-2017].

[8] MPI MorHeat pressure transmitters. Available: http://mpimorheat.com/upload/file/mpi_2012sept_24pgs_mf_melt_pressure_transducer_transmitter.pdf. [Accessed: 12-Jun-2017].

[9] SPRINGER BERLIN HEIDELBERG, 2008. Absorption and Emission of Light, in *Laser Spectroscopy*, pp. 5–60.

[10] SPRINGER BERLIN HEIDELBERG, 2008. Lasers as Spectroscopic Light Sources, in *Laser Spectroscopy*, pp. 235–396.

[11] SPRINGER BERLIN HEIDELBERG, 2008. Spectroscopic Instrumentation, in *Laser Spectroscopy*, pp. 99–233.

[12] S. BAHAA E. A. and C. T. MALVIN, 2013. Resonator, Optics, in *Fundamentals of Photonics*, 2nd ed., pp. 310–341.

[13] D. HOFSTETTER and R. L. THORNTON, 1997. Theory of loss measurements of Fabry–Perot resonators by Fourier analysis of the transmission spectra. *Opt. Lett.*, vol. 22, no. 24, pp. 1831–1833.

[14] G. C. FANG, P. G. JIA, Q. CAO, and J. J. XIONG, 2016. MEMS fiber-optic Fabry-Perot pressure sensor for high temperature application. Optical Measurement Technology and

Instrumentation, vol. 2, pp.10155 - 10159.

[15] F. PEDROTTI, L. PEDROTTI, 1993. Introduction to Optics. 2nd ed - Prentice-Hall, vol 3, pp. 234 - 261.

[16] N. N. ELKIN and A. P. NAPARTOVICH, 1994. Numerical study of the stability of single-mode lasing in a Fabry–Perot resonator with an active medium. *Appl. Math. Model.*, vol. 18, no. 9, pp. 513–521.

[17] Study of a Fabry Perot resonator. Available: https://www.researchgate.net/publication/298784956_Study_of_a_Fabry_Perot_resonator. [Accessed: 09-Jul-2017].

[18] Fresnell's Equations: Reflection and Transmission. Available: http://hyperphysics.phy-astr.gsu.edu/hbase/phyopt/freseq.html#c1. [Accessed: 31-Aug-2016].

[19] Q. YU and X. ZHOU, 2011. Pressure sensor based on the fiber-optic extrinsic Fabry-Perot interferometer. *Photonic Sens.*, vol. 1, no. 1, pp. 72–83.

[20] C. H. HUANG, G. ZHANG, Z. Q. CHEN, X. J. HUANG, and H. Y. SHEN, 2002. Calculation of the absorption coefficients of optical materials by measuring the transmissivities and refractive indices. *Opt. Laser Technol.*, vol. 34, no. 3, pp. 209–211.

[21] SPRINGER BERLIN HEIDELBERG, 2008. Widths and Profiles of Spectral Lines, in *Laser Spectroscopy*, pp. 61–98.

[22] B. J. J. SLAGMOLEN, M. B. GRAY, K. G. BAIGENT, and D. E. MCCLELLAND, 2000. Phase-sensitive reflection technique for characterization of a Fabry–Perot interferometer. *Appl. Opt.*, vol. 39, no. 21, pp. 3638–3643.

[23] G. C. HILL *et al.*, 2007. SU-8 MEMS Fabry-Perot pressure sensor. *Sens. Actuators Phys.*, vol. 138, no. 1, pp. 52–62.

[24] WARREN C. YOUNG and RICHARD G. BUDYNAS, 2012. Roark's Formulas for Stress and Strain, Eighth Edition. Available: https://accessengineeringlibrary.com/browse/roarks-formulas-for-stress-and-strain-eighth-edition. [Accessed: 30-Aug-2016].

[25] BCM Sensor Technologies, Model SE103, sensor dies for pressure applications. Available: https://www.bcmsensor.com/wp-content/uploads/2014/12/SE103_Sensor_Dies_for_Gerneral_Purpose.pdf. [Accessed: 13-Jun-2017].

[26] Thorlabs - GIF50C Graded-Index Multimode Fiber, Ø50 µm Core/Ø125 µm Cladding, 0.2 NA. Available: https://www.thorlabs.com/thorproduct.cfm?partnumber=GIF50C. [Accessed: 05-May-2017].

[27] Implantable Fiber Optic Cannulae, Ø1.25 mm Stainless Steel Ferrule. Available: https://www.thorlabs.com/newgrouppage9.cfm?objectgroup_id=6742. [Accessed: 13-Jun-2017].

[28] Implantable Fiber Optic Cannulae, Ø1.25 mm Ceramic Ferrule. Available: https://www.thorlabs.com/newgrouppage9.cfm?objectgroup_id=6741&pn=CFMLC21L20. [Accessed: 13-Jun-2017].

[29] M. BORN and E. WOLF, 1999. *Principles of Optics*. Optoelectronics and Photonics, pp. 356 - 367.

[30] A simple technique for accurate and complete characterisation of a Fabry-Perot cavity, 2013. Available: https://www.osapublishing.org/oe/abstract.cfm?uri=oe-17-24-21935. [Accessed: 16-Aug-2017].

Appendix A

SE103 Technical data sheet

Model SE103
Sensor Dies for Pressure Applications

BCM SENSOR

Technical Data

Parameters		Units	Specifications	Notes
pressure ranges	gauge	barG	0~0.1, ~0.35, ~1, ~2.5, ~4, ~6, ~10, ~16, ~25	1
	absolute/sealed gauge	barA/barS	0~1, ~2.5, ~4, ~6, ~10, ~16, ~25, ~40, ~60, ~100, ~250, ~400, ~600	1
proof pressure		%fs	200 (for ranges ⩽ 100bar); 150 (for ranges > 100bar)	2
burst pressure		%fs	300	
full scale output		mV	⩾ 60	3 & 4
excitation	voltage	Vdc	5 (typical), 1, ..., 10	
	current	mA	1 (typical), 0.2, ..., 2	
zero offset		mV	⩽ ±40	4
non-linearity (NL)		%fs	⩽ ±0.25 (standard), ⩽ ±0.5,	5
hysteresis (HY)		%fs	⩽ ±0.02	
repeatability (RP)		%fs	⩽ ±0.05	
long term stability		%fs/year	⩽ ±0.2	
short term stability		%fs/8h	⩽ ±0.1	
bridge resistance		kΩ	4~6	
storage temperature range		°C	-45 ~ +125	
operating temperature range		°C	-45 ~ +125	
temp. coeff. (TC) of bridge resistance		10^{-3}/°C	1.15 ±0.25	6
TC of zero offset		%fso/°C	0.05	7
TC of SPAN	voltage excitation	%fso/°C	0.22	7
	current excitation	%fso/°C	0.05	7
thermal HY of zero offset		%fso/°C	⩽ ±0.02	
PN junction break down voltage		V (@10μA)	⩾ 20	
dimensions	with glass constraint	mm	2.70 x 3.45 x 1.2 (⩽ 25bar), 2.45 x 2.45 x 1.2 (⩾ 40bar)	
	without glass constraint	mm	2.70 x 3.45 x 0.4 (⩽ 25bar), 2.45 x 2.45 x 0.4 (⩾ 40bar)	

Extracted from [25].